Section 1

Atmospheric data assimilation schemes, analysis and initialization, data impact studies, observing system experiments

Variational assimilation of screen-level temperature for the global semi-Lagrangian NWP model SL-AV

N.N. Bogoslovskii[2], M.A. Tolstykh[1,2]

Institute of Numerical Mathematics, RAS (1)
Hydrometcenter of Russia (2)
Moscow, Russia

e-mail: dorgun@mail.ru, tolstykh@inm.ras.ru

The parametrization of land surface processes ISBA (Interaction Soil Biosphere Atmosphere) [1] was implemented in the global semi-Lagrangian finite-difference NWP model SL-AV[2]. It is known that this parametrization is highly sensible to initial data errors of soil water content. Soil variables correction scheme consistent with the parametrization was implemented in order to improve the analysis. The scheme initializes the following surface variables: surface soil temperature, deep soil temperature, surface water content and deep soil water content. One can find the detailed description of the above scheme in [3]. Its implementation for SL-AV model is presented in [4] .

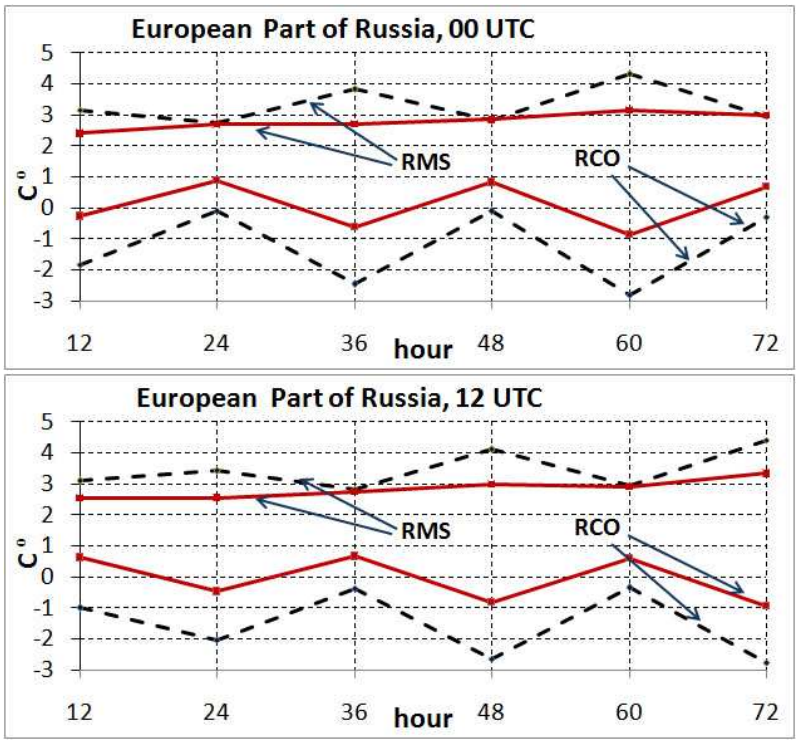

Figure 1: T_{2m} forecast errors with respect to observations. Solid lines: new analyses. Dashed lines: analyses from assimilation system of Hydrometcenter of Russia. [7]

As this scheme uses 2 meter temperature and relative humidity analysis increments, soil variables errors are influenced by screen-level analysis errors. 2D variational analysis method was implemented in order to improve screen-level temperature analysis.

Background error covariance matrix $\mathbf{B}$ is obtained using the function suggested by Tilmann Gneiting [5] with an additional term. This term takes into account orography difference between different gridpoints. 2DVAR analysis method was parallelized with OpenMP and MPI technologies.

The validation of the method was carried out in the continuous assimilation cycle. The estimates used were 2m temperature mean (RCO) and root-mean square (RMS) errors with respect

to SYNOP observations. The resolution of the model is 0.72 degrees in latitude, 0.9 degrees in longitude, 28 vertical levels. Upper-air initial fields are taken from the data assimilation system [7].

Figure 1 shows the errors of 72-hour 2-meter temperature forecast averaged for June 5-18, 2007 obtained with new analyses for soil variables, screen-level temperature and also OI relative humidity analysis [6] along with the results obtained with previously used fields from assimilation system [7]. The upper lines are root-mean square errors and the lower lines are biases. One can observe smaller screen-level temperature errors in case of using new schemes. T_{2m} forecast root-mean square error on all regions decreased on 0.6 degrees on average.

This work was supported with Russian RFFR grants No. 06-05-08109, 07-05-00893.

References

[1] Noilhan J. and Mahfouf J.-F. The ISBA land surface parameterisation scheme // Global Planet. Change, 1996, Vol 13, P. 145 - 149

[2] Tolstykh M.A. Semi-Lagrangian high-resolution atmospheric model for numerical weather prediction. // Russian Meteorology and Hydrology. 2001, є 4. P. 1 - 9

[3] Giard D. and Bazile E. Implementation of a new assimilation scheme for soil and surface variables in a global NWP model. // Mon. Wea. Rev. 2000. Vol 128, P. 997-1015

[4] Bogoslovskii N., Tolstykh M. Implementation of assimilation scheme for soil variables in the global semi-lagrangian nwp model // The Journal of Computational Technologies. 2006. Vol. 11, Special Issue ENVIROMIS-2006 Pp. 20-25. [Russian]

[5] Gneiting T. Correlation functions for atmospheric data analysis // Q.J.R. Meteorol. Soc. 1999, vol.125, P 2449-2464

[6] Shlyaeva A. and Tolstykh M. New 2-Meter Relative Humidity Analysis for SL-AV model // Research Activities in Atmospheric and Oceanic Modelling, 2008, http://collaboration.cmc.ec.gc.ca/science/wgne/

[7] Tsyroulnikov M.D., Tolstykh M.A., Bagrov A.N., Zaripov R.B. Development of a global data assimilation system with variable resolution // Russian Meteorology and Hydrology, 2008, 003, N4, pp. 5-24.

NWP preparations at Météo-France for the Concordiasi project

Aurélie Bouchard, Alexis Doerenbecher, Florence Rabier, Vincent Guidard, Fatima Karbou

Météo France/CNRM/CNRS
42 avenue de Coriolis – 31057 Toulouse- France
aurelie.bouchard@cnrm.meteo.fr

Concordiasi is an international project, currently supported by the following agencies: Météo-France, CNES, IPEV, PNRA, CNRS/INSU, NSF, NCAR, Concordia consortium, University of Wyoming, Purdue University and University of Colorado. ECMWF also contributes to the project through computer resources and support, and scientific expertise. Concordiasi is part of the THORPEX-IPY cluster within the International Polar Year effort (http://www.cnrm.meteo.fr/concordiasi/, Rabier et al., 2007). One of the main goals of this experiment is to improve the polar assimilation of IASI radiances. IASI is an advanced infrared sounder on board the European Polar orbiting satellite MetOp. From September 2008, additional conventional observations will be operated over Antarctica such as radiosoundings at the Concordia and Dumont d'Urville stations. Moreover, 600 dropsoundings will be dropped by twelve stratospheric pressurised balloons (SPB). These SPBs will be deployed from McMurdo station during two months similarly to the VORCORE campaign (Hertzog et al 2007). Figure 1 shows the trajectory of one balloon during VORCORE. During the experiment, both flight-level data (pressure, winds and temperature at 60hPa) and dropsonde data will be made available in real-time.

A daily trial will decide the deployments of sondes. Each dropsonde launch will be predicted as a function of IASI's swath, and/or the predicted meteorological sensitive area valid for that day. Figure 2 shows an example of the track of IASI over Antarctica the 7th October 2007. A sensitive area valid at 18Z that day and based on the 00Z analysis is shown in Figure 3. The verification is set on the 9th October at 00Z in the green circle. Some back-trajectories (using a simple lagrangian computation at constant pressure level) mimic the drift of some kind of SPB that would end above the main sensitive node (actually defined in the troposphere) by the targeting time (18Z). During the field phase a more realistic SPB drift model ought to be used in order to predict which SPB is likely to drop in the vicinity of a IASI swath or of a sensitive area.

As a preliminary work, the meteorological French model ARPEGE has been changed in order to have a better precision over the south polar area. This is a spectral model with a variable resolution on a stretched grid. The centre of this model has been moved southward to the Dome C station (75,12S; 123,37 E). Current resolution is then less than 35km over Antarctica. An illustration of this new geometry is shown in figure 4. An impact of this modification has been tested by estimating the difference of the observations and the guess of the model over fifteen days of simulation. A positive impact has been noted for the radiosounding observations, for the profile of temperature or zonal winds, mainly in the lower troposphere. Present and future work focuses on the polar assimilation of the infrared and micro-wave sensors (emissivity parametrisations for snow-covered areas).

References

Hertzog A., Ph. Cocquerez, C. Basdevant, G. Boccara, J. Bordereau, B. Brioit, A. Cardonne, R. Guilbon, A. Ravissont, E. Scmitt, J.-N. Valdivia, S. Venel and F. Vial, Strateole/Vorcore –

Long Duration, superpressure balloons to study the Antarctic lower stratosphere during the 2005 winter, J. Atmos; Ocean. Technol., in press, 2007.

Rabier, F., A. Bouchard, V. Guidard, F. Karbou, V-H. Pauch, N. Semane, C. Genthon, G. Picard, F. Vial, A. Hertzog, P. Cocquerez, D. Parsons, D. Barker, J. Powers, T. Hock, 2007 : The Concordiasi project over Antarctica during IPY. Joint EUMETSAT/AMS conference. Amsterdam, 24-28 September 2007

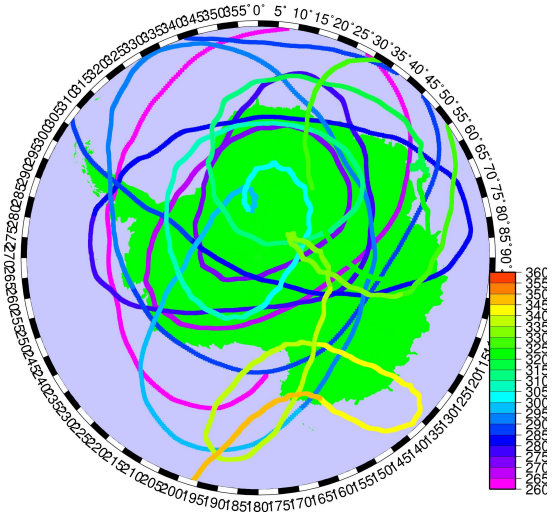

Figure 1: Trajectory of the 17th balloon during VORCORE from September to December 2005.
The colour shows the trajectory for one day.

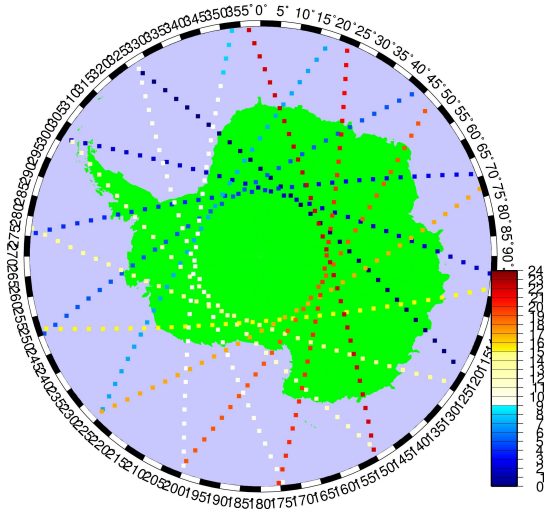

Figure 2: Track of IASI the 7th October 2007.
The colour gives the hour of the passage.

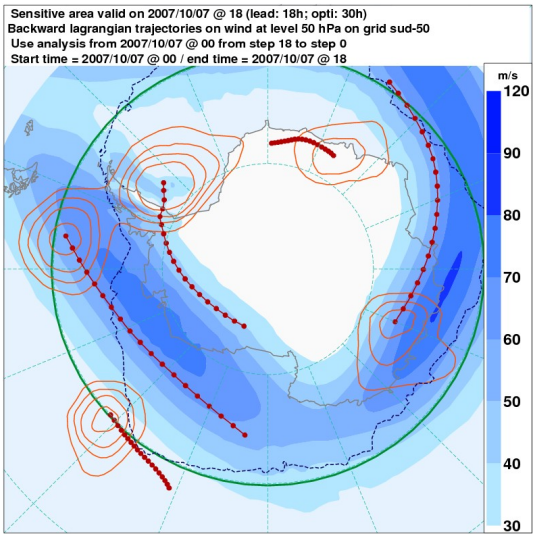

Figure 3: Predicted sensitive area valid on the 2007/10/07 at 18Z, initialized at 00Z and optimized for the 2007/10/09 at 00Z.
Balloon trajectories start on the 2007/10/07 at 00Z and reach sensitive areas at 18Z. The blue shading shows mean wind speed at 50 hPa on that period (ECMWF operational forecast). The navy dashed curve shows the limits of sea ice as in ECMWF system.

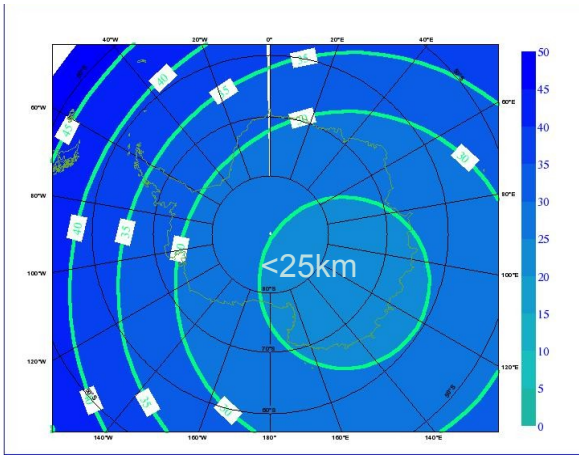

Figure 4: Horizontal resolution of the recentred model (km). A contour each 5km.

<25km

Using Isotopic Constraints to Model Monsoonal Moisture Exchange

Derek Brown and David Noone
Department of Atmospheric and Oceanic Sciences, and
Cooperative Institute for Research in Environmental Sciences
University of Colorado at Boulder, CO, USA
(email: derek.brown@colorado.edu)

The transfers of heat and moisture from the land surface to the atmosphere are substantial over monsoonal regions, yet these mechanisms are poorly resolved in current land-atmosphere models (*Dirmeyer et al*., 2006). There is a need for further understanding of the seasonal variations in the sources of moisture over monsoonal regions, including the contributions from evapotranspiration and re-evaporation of falling rain (*Henderson-Sellers et al*., 2004). Stable water isotope measurements from the Tropospheric Emission Spectrometer (TES) are useful in this regard since isotopic fractionations occurring during evaporation and condensation give rise to measurable variations in the isotopic composition of water vapor, which can be used to estimate the strength of the contributing processes. The present study uses TES isotopic values and five day back trajectories to constrain a Lagrangian isotopic exchange model that estimates the ratio of evaporative supply of water vapor to losses from precipitation (*E/P*), as well as the rainfall evaporation fraction (*F*), for the 500-825 hPa layer (*Brown et al*., 2008). Given the advection pathways from the well constrained NCEP wind fields, the isotopes allow the hydrology of the reanalysis to be tested.

Results show that very strong isotopic depletion *en route* during the wet season in the Amazon and Asian monsoon regions (**Figure 1**) exceeds that from Rayleigh distillation expectations, which can be explained by the simple rainfall evaporation model that also assumes mixing with an evaporative source. Using an oceanic source for low-level vapor, this model best fits the data using *F* values of 26% and 34% for the Amazon and Asian monsoon regional wet seasons (**Table 1**), respectively, which are consistent with the mean tropical value of 30% found by *Worden et al*. (2007). The *E*/*P* ratio of approximately 1.04 for the N. Australian wet season suggests a net gain of water from the surface to the layer 500-825 hPa, which contrasts with the stronger monsoons of the Amazon and the Asian monsoon regions. *E*/*P* estimates for the dry season indicate that supply of near-surface water vapor over the five-days prior to observation approximately balances losses due to condensation. However, the isotopic constraints in the model were only met for the Amazonian dry season when the assumed near-surface δD values were raised above the typical value of near-surface air in equilibrium with tropical ocean waters (-79‰). This anomaly suggests that the water vapor supply for the Amazon dry season is partially composed of transpired moisture.

Comparison of the best-fit *E/P* ratios with surface-based *E/P* ratios from the NCEP and ECMWF reanalyses shows reasonable agreement for the Amazon wet and dry seasons, but disagreement for both seasons of the N. Australian and Asian monsoon (which contain several oceanic grid points). These differences are largely due to large-scale subsidence which acts to increase oceanic evaporation values (via dry conditions) yet inhibit vertical transport of surface moisture to the level of the parcels (via increased stability). Future comparisons with vertical vapor flux at the 825 hPa level from the reanalysis data sets may resolve these issues.

Ultimately, this work will provide methods for spatially resolved assimilation of TES isotope data into the hydrologic cycles of monsoonal regions.

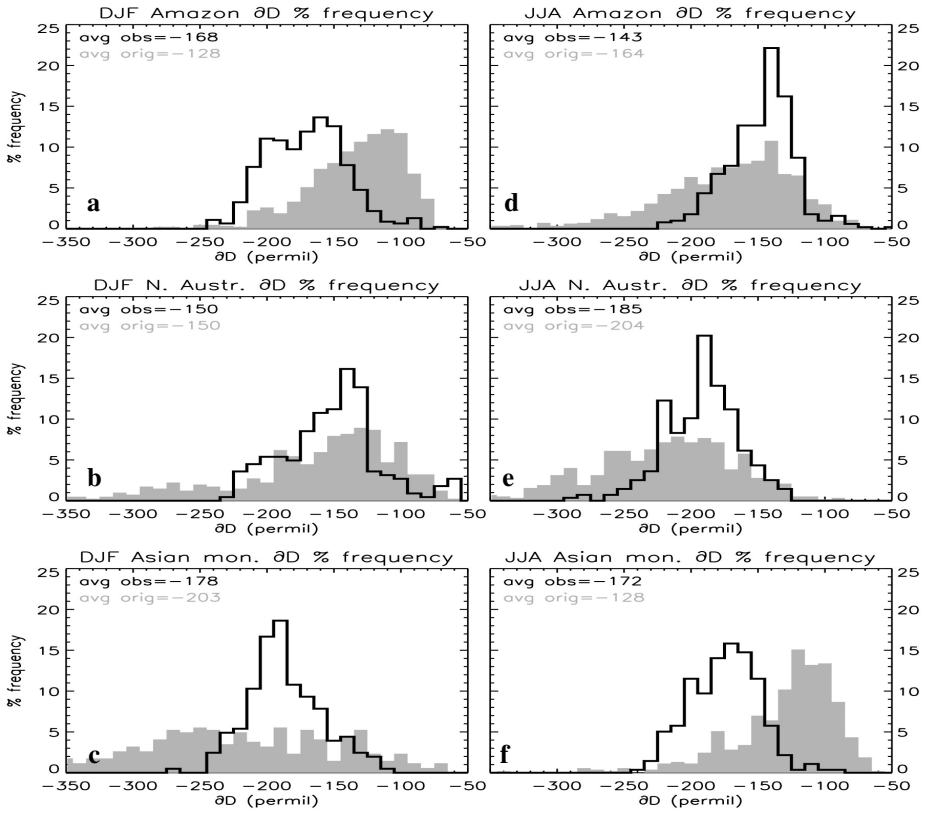

Figure 1: Frequency distribution of δD values over the layer 500-825 hPa for DJF (a,b,c) and JJA (d,e,f) seasons for the Amazon (a,d), N. Australian (b,e), and Asian Monsoon (c,f) regions. Grey shading represents δD value distribution close to the five-day back trajectory origins, while black line indicates that of the regions. Amazon= 0°S-20°S,290°-310°E, N. Australia=10°S-22.5°S,120°-140°E, and Asian monsoon=15°N -30°N,80°E-100°E.

		Oceanic source		*Continental source*		*NCEP*	*ERA*
Region	*Season*	*E/P*	*F (%)*	*E/P*	*F (%)*	*E/P*	*E/P*
Amazon	DJF	0.00 < **0.72** < 0.80	21 < **26** < 28	0.00 < **0.76** < 0.80	21 < **53** < 54	**0.63**	**0.55**
	JJA	0.94 < **0.95** < 0.95 *	00 < **00** < 03 *	0.78 < **0.86** < 0.95	00 < **28** < 45	**0.90**	**1.05**
N. Austr.	DJF	0.00 < **1.04** < 1.09	00 < **28** < 58	0.00 < **1.03** < 1.09	00 < **59** < 59	**0.63**	**0.59**
	JJA	0.87 < **0.91** < 0.96	00 < **18** < 36	0.76 < **0.94** < 0.96	11 < **62** <64	**12.9**	**13.4**
Asian mon.	DJF	0.85 < **0.88** < 0.93	00 < **06** < 25	0.69 < **0.86** < 0.93	00 < **52** < 61	**3.22**	**3.50**
	JJA	0.00 < **0.72** < 0.79	33 < **34** < 42	0.00 < **0.78** < 0.79	39 < **59** < 59	**0.42**	**0.30**

Table 1: Modeled rainfall evaporation fractions and ratios of net evaporation to net precipitation over the five-day transport pathways. Model was run for both an oceanic source, with a δD source value of the near-surface air of -79‰, and for a continental source with δD value of the source vapor set to that of regional precipitation (deduced from GNIP). Bold indicates best fit, while range indicates valid output using the constraint that modeled δD must be within one standard deviation of the mean regional δD values. Asterisk indicates that model constraints could only be met with δD source value greater than -65‰, and so the source can not be purely oceanic (-79‰).

References

1. Brown, D., J. Worden and D. Noone (2008), Comparison of atmospheric hydrology over convective continental regions using water vapor isotope measurements from space, submitted to Journal of Geophysical Research – Atmospheres, December, 2007.

2. Dirmeyer, P.A., R.D. Koster, and Z. Guo (2006), Do global models properly represent the feedback between land and atmosphere?, *J. Hydrometeor., 7*, 1177-1198.

3. Henderson-Sellers, A., K. McGuffie, D. Noone, and P. Irannejad (2004), Using Stable Water Isotopes to Evaluate Basin-Scale Simulations of Surface Water Budgets, *J. Hydrometeor.*, *5*, 805–822.

4. Worden J, D. Noone, K. Bowman, et al. (2007), Importance of rain evaporation and continental convection in the tropical water cycle, Nature, *445*(7127), 528-532, doi:10.1038/nature05508

A New 4D-Var for Mesoscale Analysis at the Japan Meteorological Agency

Yuki Honda and Ken Sawada
Numerical Prediction Division, Japan Meteorological Agency
1-3-4 Otemachi, Chiyoda-ku, Tokyo 100-8122, JAPAN
(e-mail: honda.yuuki@met.kishou.go.jp)

1. Introduction

The Japan Meteorological Agency (JMA) has operated a mesoscale numerical weather prediction system, the Mesoscale Analysis and Mesoscale Model (MSM), for disaster prevention and aviation forecast since March 2001. The current operational mesoscale analysis system is a four-dimensional variational data assimilation system (Meso 4D-Var), which has been used since March 2002 (Ishikawa and Koizumi 2002). A hydrostatic spectral model was adopted as a time integration operator in the Meso 4D-Var. Although this model used to be a forecast model of MSM, it was replaced with a fully-compressible nonhydrostatic grid model (JMA-NHM) in September 2004 (Saito et al. 2006). Since the analysis by a 4D-Var is optimized for an adopted forecast model, it is desired to adopt the same forecast model for the forecast and the analysis. For this reason, a new JMA-NHM based four-dimensional variational data assimilation system, JNoVA, has been developed (Honda et al. 2005). In 2008, the Meso 4D-Var will be replaced with this JNoVA.

2. Specifications of the new Mesoscale Analysis (JNoVA)

The detailed specifications of the JNoVA are described in Honda et al. (2005). The main modifications of the JNoVA after Honda et al. (2005) are the introduction of the incremental formulation (Courtier et al. 1994) and the new control variables based on Barker et al. (2004). The differences between the JNoVA and the Meso 4D-Var are listed in Table 1. The analysis is performed every 3 hours. Since the data assimilation window of the Meso 4D-Var is 6 hours, the former 3 hours are overlapped with the latter 3 hours of the previous data assimilation window. Although the observation data assimilated in the previous analysis are not used in the next analysis, the data reported after the data cut off time of the previous analysis are assimilated in the next analysis. So more observation data are assimilated in the Meso 4D-Var than the JNoVA. Besides this, the length of the assimilation window and the iteration number are also advantageous to the Meso 4D-Var. Meanwhile, the resolution of the JNoVA is higher than that of the Meso 4D-Var.

Table 1: The difference between the Meso 4D-Var and the JNoVA

	Meso 4D-Var	JNoVA
Adopted Forecast Model	Hydrostatic Spectral Model	Nonhydrostatic Grid Model (JMA-NHM)
Balance of Control Variables	Geostrophic Balance with Surface Friction	Nonlinear Balance (Barker et al. 2004)
Penalty Term	Suppress Time Tendency of Divergence	Incremental Digital Filter
Resolution:Outer/Inner/Layers	10km / 20km / 40layers	5km / 15km / 40layers
Data Assimilation Window	6hours	3hours
Iteration Number	40 –60 times	30 times

3. Performance of the JNoVA

To compare the performance of the JNoVA with that of the Meso 4D-Var, the experimentation has been conducted under almost the same conditions to the operational system in summer (2004/8/1 ~ 8/31) and in winter (2005/12/19 ~ 2006/1/15).

From the verification using the upper-air observation and the surface observation, the accuracy of the wind forecast of the JNoVA is the same as that of the Meso 4D-Var. As for the temperature and the humidity, the lower atmosphere of the JNoVA becomes cooler and moister than that of the Meso 4D-Var, so that the mean errors of the temperature and the humidity are improved in both seasons (Fig. 1). Their root mean square errors (RMSEs) are also reduced in winter although they are degraded in summer (not shown). In winter, the RMSEs of the surface variables of the temperature and the dew point of the analysis by the JNoVA are also well improved (not shown).

Fig.2 shows the score of the quantitative precipitation forecast (QPF) of 3 hourly accumulated precipitation (RR3).

In winter, the QPF of the JNoVA is better than that of the Meso 4D-Var in the range of RR3 ≤ 5mm. Although the score of RR3 ≥ 10mm of the JNoVA is worse than that of the Meso 4D-Var, the ratio of the occurrence of RR3≥ 10mm is less than 5% of all RR3. Most of the precipitation in winter is snow and RR3 is less than 5mm. On the other hand, the score is almost the same in summer although the performance of RR3 ≤ 5mm is a little degraded. This is because the QPF of the JNoVA tends to spread the precipitation area of the weak rain.

In general, the JNoVA shows the similar performance to the Meso 4D-Var and the forecast of the JNoVA sometimes shows better results than that of the Meso 4D-Var (Fig.3). However, the degradation of the QPF is a crucial problem. After resolving this problem, the JMA will replace the Meso 4D-Var with the JNoVA in 2008.

The horizontal resolution of the analysis of the JNoVA is twice higher than that of the Meso 4D-Var. Besides, it would reduce the development cost of the MSM since the same forecast model, JMA-NHM, is used in forecast and analysis. These factors would be benefits of this upgrade of the operational mesoscale analysis system.

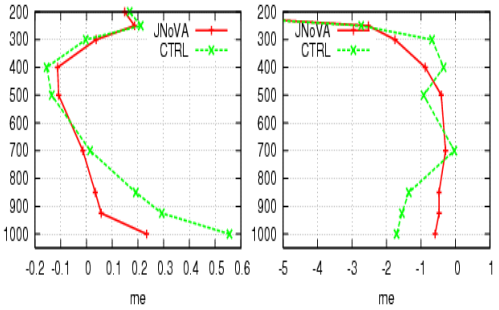

Fig. 1: Mean error of temperature (left) and relative humidity (right) of 3 hour forecast.

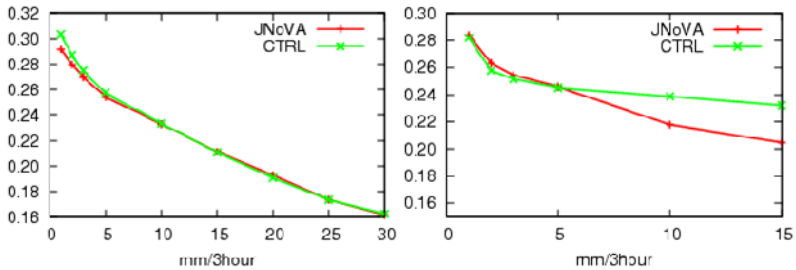

Fig. 2: Equitable threat score of 3hourly accumulated precipitation forecast in summer (left) and winter (right). The red and green line shows the results of the JNoVA and the Meso 4D-Var (CTRL), respectively. The horizontal axis is the threshold value of the rainfall amount.

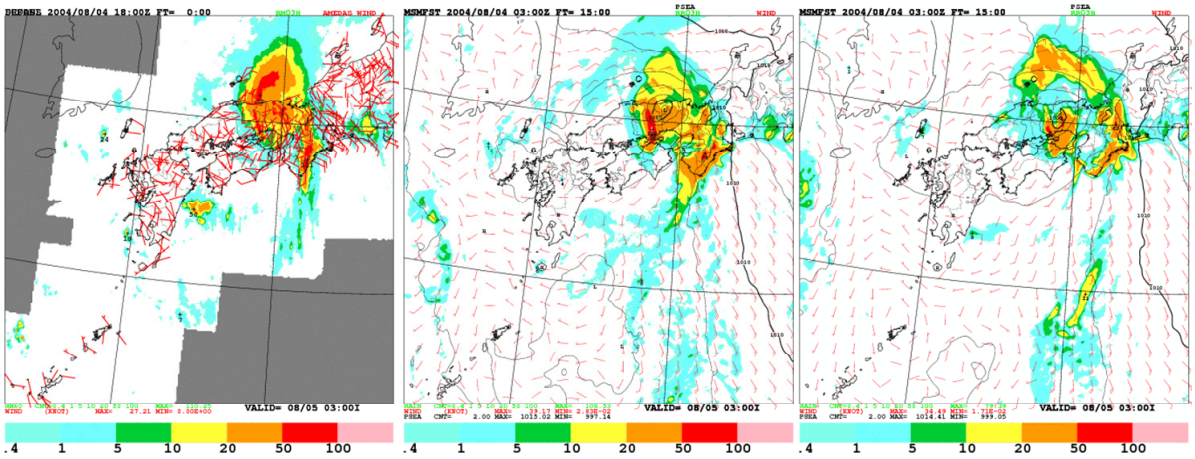

Fig. 3: 3 hourly accumulated rainfall of QPE (Radar-raingauge Analyzed Precipitation) (left), 15-hour forecast from the initial field analyzed by the JNoVA (middle) and that from the initial field by the Meso 4D-Var. The initial time is 03 UTC on 4th August, 2004.

References

Barker, D.M. et al., 2004: A three dimensional variational data assimilation system for MM5: Implementation and Initial results. *Mon. Wea. Rev.*, **132**, 897-914.

Courtier et al. 1994: A strategy for operational implementation of 4D-Var, using an incremental approach. *Q. J. R. Meteorol. Soc.*, **120**, 1367-1387.

Ishikawa, Y. and K. Koizumi, 2002: Meso-scale Analysis. *Outline of the Operational Numerical Weather Prediction at the Japan Meteorological Agency*, 26-31.

Saito, K., et al., 2006: The operational JMA non- hydrostatic mesoscale model. *Mon. Wea. Rev.*, **134**, 1266-1298.

Honda, Y., et al., 2005: A pre-operational variational data assimilation system for a non-hydrostatic model at the Japan Meteorological Agency: Formulation and preliminary results. *Q. J. R. Meteorol. Soc.*, **131**, 3465-3475.

Assimilation of WV CSR from MTSAT-1R in the JMA global 4DVAR system

Toshiyuki Ishibashi
Numerical Prediction Division, Japan Meteorological Agency
1-3-4 Otemachi, Chiyoda-ku, Tokyo 100-8122, JAPAN
E-mail: ishibasi@met.kishou.go.jp

JMA has been operationally using the clear-sky radiances of the water vapor channel (WV CSRs) from MTSAT-1R in the JMA global four dimensional variational (4DVAR) data assimilation system since 7 June 2007. WV CSRs are generated by averaging radiances of cloud-free pixels in 16 x 16 pixels (60 km x 60 km at nadir). WV CSRs have information on the middle and upper tropospheric humidity.

Several quality control procedures are applied to WV CSR data before the assimilation in 4DVAR. The data are thinned to 2.0 degrees horizontally and every two hours temporally. Those having a low percentage of clear pixels, a large standard deviation of brightness temperature, or a large departure (observation minus first-guess) are excluded. A variational bias correction scheme (Sato 2006) is applied in the 4DVAR system.

Observing System Experiments were carried out to evaluate the impacts of WV CSR on both analysis and forecast quality in August 2006 and January 2007. Adding WV CSR slightly reduced dry biases of the first-guess and analysis with respect to the radiosondes in the mid troposphere in the Tropics and the Southern Hemisphere. In the boreal summer experiment, the root mean square errors (RMSEs) of forecasts were reduced by assimilating WV CSR with respect to the analyses for the 500 hPa geopotential height in the Tropics and the Northern Hemisphere, and for the 850hPa temperature in the Tropics and South Hemisphere (Fig. 1). The cold temperature biases at 850hPa in the global areas were also improved (Fig. 2). Typhoon track forecast errors were clearly reduced (Fig. 3). In the boreal winter experiment, the RMSEs were reduced for the 500 hPa geopotential height and the 850hPa zonal wind velocity in the Tropics (data not shown).

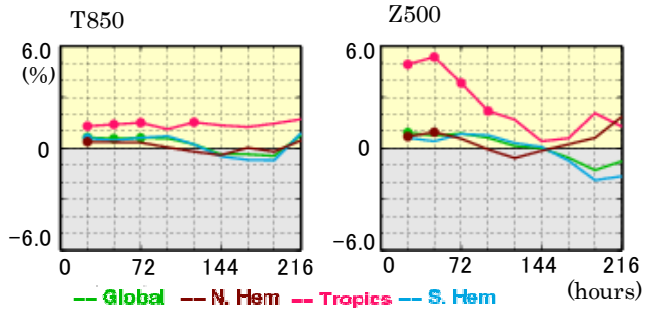

Fig.1. Improvement Rate of RMSE of Forecast (IRRF) for 850hPa temperature and 500hPa geopotential height. IRRF is defined as follows:
IRRF= (RMSEcntl − RMSEtest)/ RMSEcntl.
Dots on these score lines represent statistical significance.

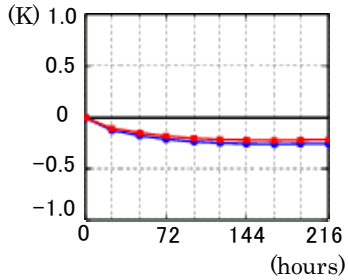

Fig.2. Temperature biases at 850hPa in the global areas for the cases with WV CSR (red line) and without WV CSR (blue line).

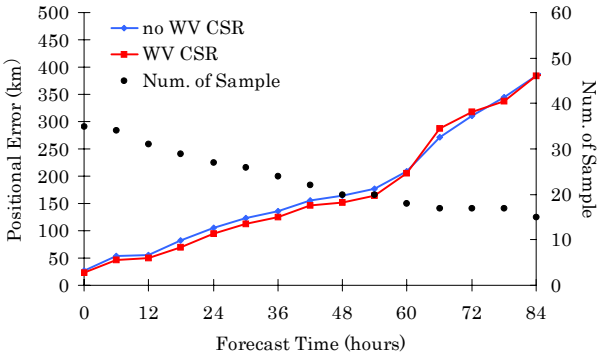

Fig.3. Typhoon track forecast errors of the run with WV CSR (red line) and without WV CSR (blue line) in August 2006. The dots represent the sample size.

Reference:
Sato, Y, 2006: Introduction of variational bias correction technique into JMA global data assimilation system. *CAS/JAC WGNE Research Activities in Atmospheric and Oceanic Modelling*, **37**, 1-19.

Towards the assimilation of surface sensitive satellite microwave observations over land at Météo-France

Fatima Karbou, Élisabeth Gérard, Florence Rabier

CNRM/GAME, Météo-France/CNRS, 42 Av. Coriolis, 31057 Toulouse, France
fatima.karbou@meteo.fr

Satellite microwave measurements have large atmospheric and surface information contents and are known to be very useful for Numerical Weather Prediction. However these observations are still not fully used over land because of non negligible uncertainties about land emissivity and surface temperature. Recent developments have been carried out at Météo-France in order to propose new methods for land emissivity and surface temperature modelling anchored on satellite microwave observations. The methods, fully described in Karbou *et al.* (2006), have been interfaced with the RTTOV model. (1) The first method is based on the use of averaged emissivity estimates calculated within the assimilation system two weeks prior to the assimilation period; (2) the second one uses dynamically varying emissivities derived at each pixel using one surface channel or a selection of surface channels, and (3) finally the third method combines the two previous ones since it uses averaged emissivities and dynamically estimated skin temperature at each pixel using observations from one surface channel.

The relevance of the use of the new methods to assimilate microwave observations over land has been investigated using AMSU-A, AMSU-B and SSM/I observations. The performances of the three methods have been studied in terms of observation departures from first guess and analysis and also in terms of analysis and forecast impacts. So far periods of test have been chosen around the August-September 2005 and 2006 AMMA periods (African Monsoon Multidisplinary Analyses, Redelsperger *et al.*, 2006; Parker *et al.*, 2008). The results show that an important amount of data is assimilated when the land surface emissivity and/or the surface temperature is updated. Even sounding channels that receive a lesser contribution from the surface take advantage of this modification (see Figure 1). The assimilation of surface sensitive channels over land with improved land surface characteristics modelling appears to have a strong impact on the hydrological cycle both in analysis/first guess and short to medium range forecast and is globally beneficial to our analysis and forecast system.

The 2005 experiments show that assimilating AMSU surface sensitive channels over land leads to a moistening in the Tropics and Southern Hemisphere (mainly over sea) and a drying in the Northern Extratropics (mainly over land). Globally similar effects are induced by the three land emissivity / surface temperature schemes, with local differences, as for example, over half North of Africa where the drying – associated to a strong reduction of precipitation - is maximum with the second method (dynamic computation of emissivity), as shown in Figure 2. As a result, the ITCZ moves towards the South, which is an encouraging feature (especially for the AMMA community) as our model usually suffers from spurious heavy rain rates in this region. Very similar results to those obtained with AMSU data have been found when assimilating SSM/I channels over land. The impact on forecast skills is globally neutral to positive for geopotential, temperature and humidity. Differences in the response of each of the methods are noticeable but more investigation is needed to decide between them for an operational implementation. These results should be considered as preliminary results and need to be re-evaluated in the light of other developments, such as the variational bias correction (VarBC) as developed at ECMWF (Dee, 2005; Auligné *et al*., 2007) – ongoing experiments under evaluation -, the tuning of observation error over land and the introduction of error correlation between channels.

References

Auligné, T., McNAlly, A.P. and Dee, D., 2007: Adaptive bias correction for satellite data in numerical weather prediction system. *Q. J. R. Meteorol. Soc*., **133**, 631-642

Dee, D.P., 2005: Bias and data assimilation. *Q. J. R. Meteorol. Soc*., **131**, 3323-3343

Karbou, F., Gérard, É. and Rabier, F., 2006: Microwave land emissivity and skin temperature for AMSU-A and –B assimilation over land. *Q. J. R. Meteorol. Soc*., **132**, 2333-2355

Parker, D.J., Fink, A., Janicot, S., Ngamini, J.-B., Douglas, M., Afiesimama, E., Agusti-Panareda, A., Beljaars, A., Dide, F., Diedhiou, A., Lebel, T., Polcher, J., Redelsperger, J.-L., Thorncroft, C., Ato

Wilson, G., 2008: The AMMA radiosonde program and its implications for the future of atmospheric monitoring over Africa. *Bull. Am. Met. Soc*., submitted

Redelsperger, J-L., Thorncroft, C. D., Diedhiou, A., Lebel, T. , Parker, D. J. and Polcher, J., 2006: African Monsoon Multidisciplinary Analysis: An International Research Project and Field Campaign. *Bull. Am. Met. Soc.*, **87**, 1739-1746

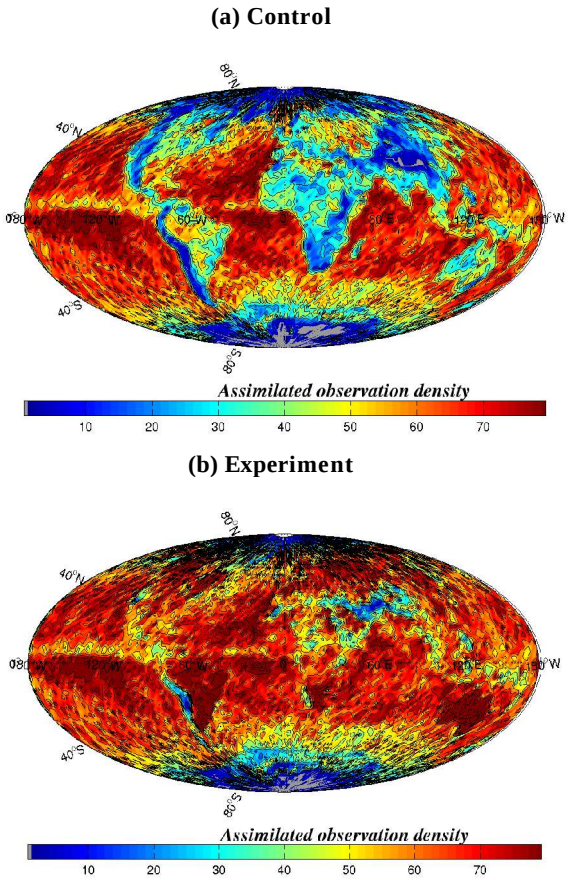

Figure 1*:* Density of assimilated observations (number of assimilated observations over a 2°x2° grid) from AMSU-A channel 7 and over August 2006. Results are given for (a) the control and for (b) an experiment that uses dynamically varying emissivities derived at AMSU-A channel 3.

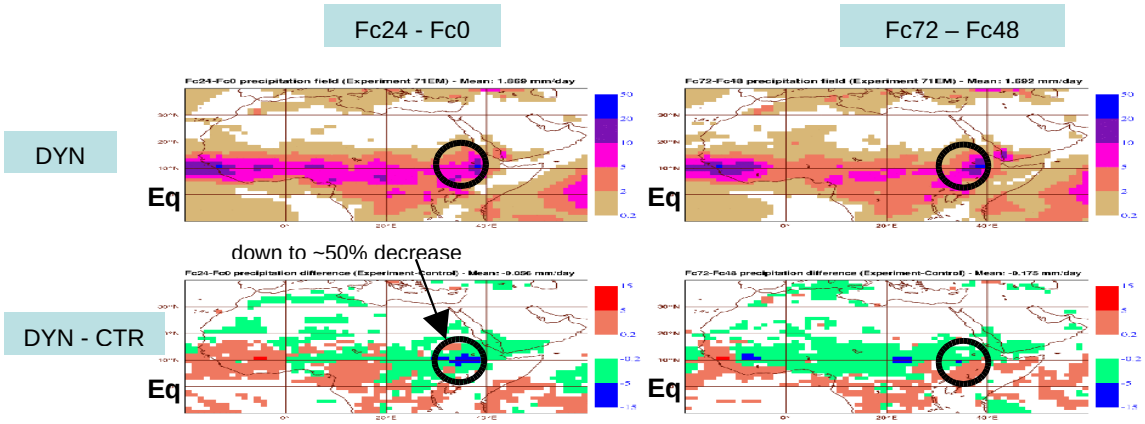

Figure 2*:* Mean 24-hour cumulated precipitation field (15 August-3 September 2005) over half North of Africa at day 1 (left panels) and day 3 (right panels) forecast ranges for the experiment using surface sensitive channels over land based on method 2 (top panels) and the difference between this experiment and the reference run (without AMSU surface sensitive channels over land) (bottom panels). Units are in mm.day^{-1}.

An Assimilation Experiment of a Heavy Rainfall Event around Tokyo with a Cloud-Resolving Nonhydrostatic 4D-Var Assimilation System

Takuya KAWABATA, Tohru KURODA, Hiromu SEKO, Kazuo SAITO
(Meteorological Research Institute / Japan Meteorological Agency)

1. Introduction

The Forecast Research Department of the Meteorological Research Institute (MRI) has been developing a high-resolution nonhydrostatic 4 dimensional variational assimilation system (NHM-4DVAR) based on the Japan Meteorological Agency nonhydrostatic model (JMA-NHM). The aim is to apply a 4DVAR technique to the mesoscale convective cloud system with a cloud resolving resolution less than 2 km. NHM-4DVAR was applied to a heavy rainfall event occurred at Tokyo on 21 July 1999 (Kawabata et al. 2007), and the NHM-4DVAR quantitatively well reproduced compared with the observations. In this case, perturbations to the dry dynamics and the advection of water vapor are considered in the NHM-4DVAR, and the Doppler Radial Wind (RW) data, GPS precipitable water vapor (GPS-PWV) data, surface wind and surface temperature data were assimilated. After this successful result, the NHM-4DVAR has been modified further in order to assimilate the radar reflectivity data, and an assimilation experiment has been underway for the heavy rainfall event around Tokyo on 4-5 September 2005.

2. NHM-4DVAR

A forward model of NHM-4DVAR is a full nonlinear JMA-NHM, while a tangent linear and an adjoint model consider perturbations to the dynamics and the warn rain cloud microphysics process. Control variables are horizontal wind (u, v), vertical wind (w), nonhydrostatic pressure, potential temperature, surface pressure and total water (mixing ratios of water vapor + cloud water), rain water / saturation pressure of water vapor. Last two variables are new control variables to introduce perturbations to the water substances to the NHM-4DVAR. These are chosen in consideration of the characteristics of their error statistics and the correlation with other variables.

The Z-Qr relation (eq.1, Sun and Crook 1997) is adopted as the observation operator for the assimilation of the radar reflectivity data. Because the Z-Qr operator is linear equation, it is better than other operators. The observational error is set to 15 dBZ. This value is much larger than the measurement error of the radar. In general, the observational error includes the measurement error, the representativeness error and the conversion error. Furthermore conversion error is consists of the error of the model error and the observation operator. Since only warm rain cloud microphysical process is implemented to the adjoint model and the observation operator does not include the effect of the snow, hail and graupel, the conversion error is considered large.

$$Z_{qr} = 10 \times \log 10\left(cqr \times \left(dns \times qr\right)^{1.75}\right) \qquad (1)$$

3. Assimilation experiment

NHM-4DVAR was applied to a heavy rainfall event around Tokyo on 4-5 on September 2005. The assimilation area is about 240 km x 240 km which covered the Kanto plain on the middle part of Japan Island. The assimilation window is set to 10-minutes during 20-21 JST on 4 Sep. 1-hour assimilation window was conducted in the heavy rainfall event described above, while it is not available in this case, because of the nonlinearity. 6 assimilation windows were conducted during 1 hour and the results were compared with the observations.

The Radial Wind data (RW) and the radar reflectivity derived by the Doppler radars, the GPS Precipitable Water Vapor (PWV) data and the surface observation data are available as the high temporal and spatial resolution data. In NHM-4DVAR, RW data and the reflectivity data are assimilated with 1 minute interval by every elevation angle and both data from 0.7 to 5.4 degree elevation angle are used for assimilation to remove undesirable high elevation angle data. GPS-PWV data are assimilated with 5 minutes interval, and the surface wind and temperature data observed by the Automated Meteorological Data Acquisition System (AMeDAS) of JMA are assimilated with 10 minutes interval.

Figure 1 shows the comparison of radar reflectivity (dBZ) between the observations and

the analysis. The locations, horizontal size and the intensity of the main rain band are well reproduced compared with the observations. Except for the main rain band, another convective cell easterly located on the main rain band is also reproduced. The rainfall intensity is shown in Fig. 2. As well as the reflectivity, the precipitaion intensity is well reproduced. The agreement of the reflectivity fields shows that the assimilation procedure works well. On the other hand, the agreement of the precipitaion intensity fields shows that the structure of the rain band is basically reproduced.

4. Assimilation of “0 dBZ”

The numerical models often produce false precipitation in their simulation. If “0 dBZ” observations are assimilated at the false precipitation area, these areas will be eliminated in the assimilation result and the forecast fields will be improved. But this method includes some troubles. On the one point of view, small reflectivity is not clear that these are reflected by rain water. Consequently, only the reflectivity over 10 dBZ is assimilated in the NHM-4DVAR. On the another point of view, assimilation of “0 dBZ” provides the result that most convections in the assimilation area are eliminated, because the number of grids of “0 dBZ” is much larger than one of “over 10 dBZ” in the assimilation field and the costfunction converges to the “0 dBZ” field. To deal these problems, we introduce following method: If the reflectivity is over 10 dBZ in the first guess field and under 10 dBZ in the observations, the grid is regarded as the false precipitation to be eliminated, and “0 dBZ” observations are assimilated. The observational error of “o dBZ” is set to 4 times of the normal one, because “0 dBZ” is not real observations. Result is shown in Fig. 3.

5. Conclusion

A cloud-resolving nonhydrostatic assimilation system with warm rain cloud microphysics called NHM-4DVAR, was developed. The system was applied to a heavy rainfall event and reproduced observed rain band both in the reflectivity and the rainfall intensity. “0 dBZ” assimilation technique was introduced to the NHN-4DVAR.

References

Kawabata, T., H. Seko, K. Saito, T. Kuroda, K. Tamiya, T. Tsuyuki, Y. Honda, Y. Wawazuki, 2007: An Assimilation and Forecasting Experiment of the Nerima Heavy Rainfall with a Cloud-Resolving Nonhydrostatic 4-Dimensional Variational Data Assimilation System, *JMSJ*, **85**, 255-276

Sun and Crook, 1997: 1997: Dynamical and microphysical retrieval from Doppler radar observations using a cloud model and its adjoint. Part I: Model development and simulated data experiments. *J. Atmos. Sci.*, **54**, 1642–1661.

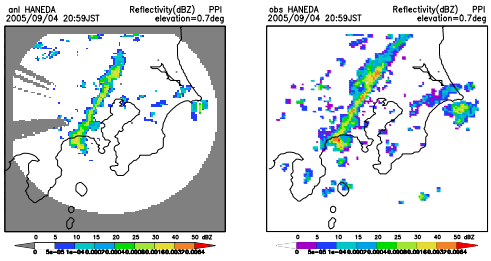

Fig. 1 Radar reflectivity(dBZ). Left: assimilation. Right: observation.

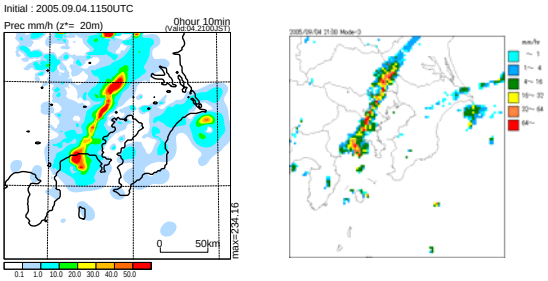

Fig. 2 Precipitaion intensity(mm/h). Left: assimilation. Right observation.

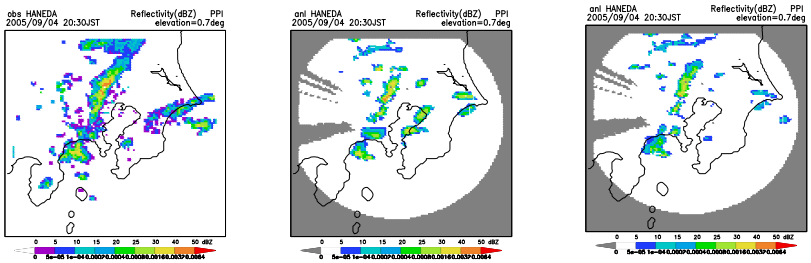

Fig. 3 Assimilation “0 dBZ”. Left: observation. Middle: first guess. Right:assimilation.

Assimilation of Precipitation Data in Beijing Area

Masaru Kunii, Kazuo Saito, Hiromu Seko

Meteorological Research Institute, Tsukuba, Ibaraki 305-0052, Japan; mkunii@mri-jma.go.jp

The Meteorological Research Institute (MRI), collaborating with JMA, participates in the WWRP Beijing Olympic 2008 Research and Development Project (B08RDP). In this project, we developed the mesoscale ensemble system (MEPS), in which the JMA non-hydrostatic model (NHM) with a horizontal resolution of 15km (Saito *et al*. 2008) was employed. In a preliminary experiment conducted in 2006 and 2007 for B08RDP, the JMA operational regional analysis, which covers forecast domain of B08RDP, supplied initial condition of the control run. But in last November the regional analysis was replaced to the global analysis system, which has horizontal resolution of about 80km at the increment calculation of 4D-Var. To assimilate observation data without much thinning and to prepare accurate and high-resolution initial fields, the JMA operational meso-scale analysis system is modified so as to permit its use in China area.

Meso-scale analysis system is designed for the JMA meso-scale hydrostatic model. The domain of this system is 3600km×3200km over Beijing and 40 vertical levels up to 10hPa. Incremental method is used in the iteration of 4D-Var to save computational time, so inner model has 20km horizontal resolution, which is lower than outer model's 10km resolution. Assimilation window length is 3-hour, and observational data are collected into 1 hour time slot and assimilated 4 times in the window. Assimilated observational typical data are radiosonde, pilot balloon, wind profiler, aircraft, ship buoy, and Radar-AMeDAS analyzed rainfall. The satellite data such as, SSM/I, TMI, AMSR-E are also assimilated as retrieved one-hour precipitation amount and total precipitable water. And QuickSCAT sea surface wind can be assimilated. In this system, 3 hour rainfall amount observed by rain gauge data over China and 1 hour rainfall amount of STEPS (Bowler *et al.* 2006) data around Beijing area (500km×500km) are assimilated additionally. The rain gauge data are processed by averaging and interpolating before assimilation (Fig.1). These precipitation data are assimilated following the work of Koizumi *et al.* (2005). Because the initial time of B08RDP experiment is 12UTC, the assimilation cycle starts at 06UTC and the analysis field of 12UTC is utilized for initial condition of the control run.

Fig.2 shows the threat scores for 6-hour accumulated precipitation forecasts against the rain gauge observation over China. Verification period is 13 days from 25 July 2007. Meso-scale analysis is inferior to regional analysis to some extent because observation data during the 3-hour period just after the initial time are assimilated additionally in regional analysis. With rain gauge data assimilated, the threat score is slightly superior to others (Fig.2 (a)). Furthermore we can see STEPS analysis data also improve the forecast (Fig.2 (b)). But unnatural precipitation near the radar site was observed several times during test period, quality control of the observations is necessary to make better analysis fields.

Acknowledgement

We acknowledge the STEPS data which are by courtesy of Dr. Alan Seed of BMRC.

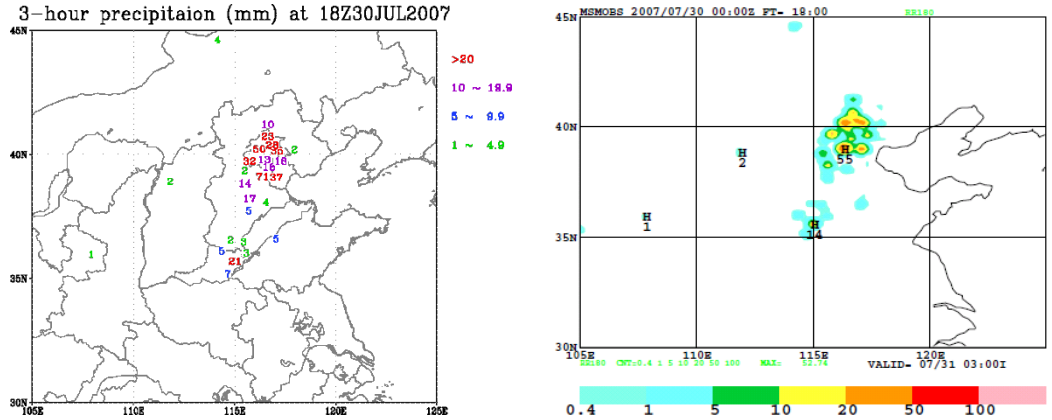

Fig.1. 3-hour accumulated precipitation data at 18UTC 30 July 2007. (a) rain gauge observations over China. (b) Processed assimilation data from rain gauge observations.

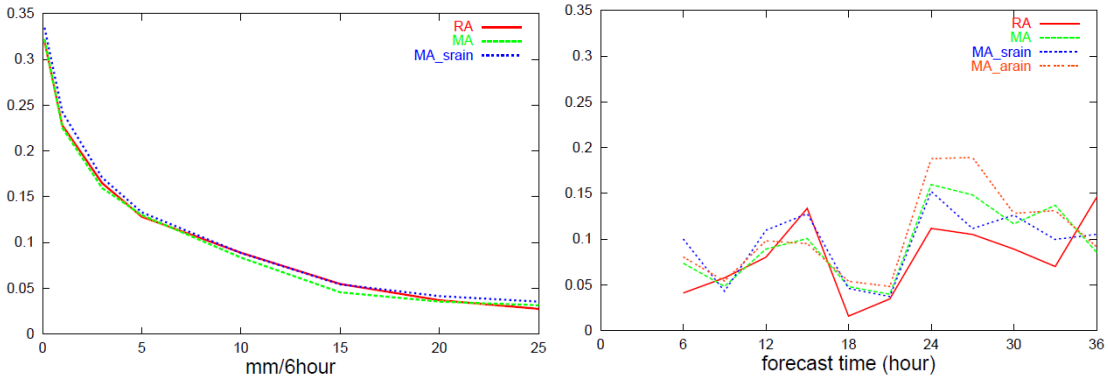

Fig.2. Threat score for 6-hour precipitation forecast against the rain gauge observation over China. Verification period is 13 days from 25 July 2007 (RA; regional analysis, MA; meso-scale analysis, MA_srain; meso-scale analysis with 3-hour accumulated rain gauge data, MA_arain; meso-scale analysis with STEPS analyzed rain data). (a) Verified in the domain of the common verification area (105°E-125°E, 30°N-45°N) of B08RDP (b) Threshold is 3.0mm/6hour and verified in the domain of STEPS data.

References

Saito, K. H. Seko, M. Kunii, M. Hara, T. Hara and M. Yamaguchi, 2008: Mesoscale Ensemble Prediction experiment for WWRP Beijing Olympic 2008 RDP -- 2007 preliminary experiment -- *CAS/JSC WGNE Research Activities in Atmospheric and Oceanic Modelling*. **38**. (submitted)

Bowler, N.E., Pierce, C.E., Seed, A.W., 2006: STEPS: A probabilistic precipitation forecasting scheme which merges an extrapolation nowcast with downscaled NWP. *Q. J. R. Meteorol. Soc.*, **132**, 2127–2155.

Koizumi, K., Y. Ishikawa, T. Tsuyuki, 2005: Assimilation of Precipitation Data to the JMA Mesoscale Model with a Four-dimensional Variational Method and its Impact on Precipitation Forecasts. *SOLA*, Vol.**1**, 45-48.

Developments of a local ensemble transform Kalman filter with JMA global model

Takemasa Miyoshi*†, Yoshiaki Sato**, Takashi Kadowaki*, Masahiro Kazumori*,
Ryota Sakai*, and Munehiko Yamaguchi*
*Numerical Prediction Division, Japan Meteorological Agency
**Environmental Modeling Center, National Centers for Environmental Prediction, NOAA

Miyoshi and Sato (2007) reported their successful implementation of the local ensemble transform Kalman filter (LETKF, Hunt et al. 2007) with the JMA global model (GSM). They also succeeded in assimilating satellite radiances, which indicated positive impact. After the report by Miyoshi and Sato (2007), the following major upgrades have been made to the GSM-LETKF system:

1) Removing local patches as in Miyoshi et al. (2007)
2) Applying an additive covariance inflation method as in Whitaker et al. (2007), but using JRA-25 (Onogi et al. 2007) instead of NCEP/NCAR reanalysis (Kalnay et al. 1996)
3) Applying an efficient parallel algorithm
4) Applying an adaptive bias correction for satellite radiances to simulate the operational variational bias correction within 4D-Var (Sato 2007)

The details are described in a separate paper, which is in preparation at the moment. This short report presents recent results of the comparison between LETKF and the JMA operational 4D-Var (Kadowaki 2005) and ensemble prediction system (EPS).

LETKF performed well in typhoon track forecast. The typhoon Rananim case in 2004 showed an excellent performance of LETKF (Fig. 1). LETKF captured the westward movement successfully, although most operational systems at that time predicted the northward movement, leading to false caution to Japan. Even with JMA's latest operational EPS with singular vectors centered at 4D-Var analysis (Sakai et al. 2008), just a few ensemble members out of 51 captured the westward movement. Not just in this case but on average over many cases, we obtained improvements of the track forecast.

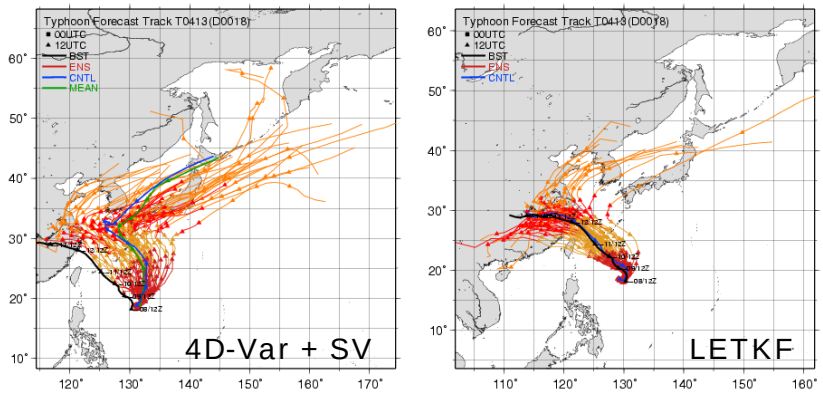

Fig. 1. 51-member typhoon track ensemble forecast in the typhoon Rananim case initialized at 12 UTC 8 August 2004. Left and right panels indicate operational singular-vector ensemble prediction system centered at 4D-Var analysis and LETKF, respectively. The thick black line indicates the best track. The red/orange lines indicate ensemble members. The blue and green lines show control forecast and ensemble mean, respectively.

To make an overall comparison between LETKF and 4D-Var, forecast anomaly correlations are compared; Figure 2 shows the relative improvements of LETKF over 4D-Var. Without the adaptive bias correction for satellite radiances, high temperature bias existed in the LETKF analysis, which leads to large degradation of forecasts. This problem was found to be caused by the fact that RTTOV-8 has been applied to LETKF rather than RTTOV-7 which is used in the operational 4D-Var and quality control systems. It turned out that the surface emissivity model FASTEM-2 of RTTOV-7 contained some known bugs causing spurious positive bias in the calculated surface emissivity. As a result, radiances are computed to be spuriously large for satellite sensors sensitive to the surface emissivity such as AMSU-A ch.4, which are also sensitive to the lower tropospheric temperature. Therefore, the observations are too

† Corresponding author address: Numerical Prediction Division, Japan Meteorological Agency, 1-3-4 Otemachi, Chiyoda-ku, Tokyo 100-8122, Japan. E-mail: miyoshi@naps.kishou.go.jp

low compared to the computed radiances; the variational bias correction scheme in 4D-Var adds positive value to the observation to remove the biased differences. Without the adaptive bias correction within LETKF, the same bias correction has been applied. However in LETKF, RTTOV-8 does not contain the bugs in FASTEM-2. Therefore, the observations after the "wrong" bias correction are too high, which results in the high temperature bias in the lower troposphere.

After applying the adaptive bias correction, the estimated bias was drifted rapidly away from the optimal value for 4D-Var; it happened only to the satellite channels sensitive to the surface emissivity. Then, we obtained much improvement as shown in Fig. 2 (b). However, the positive bias in the analysis was not completely removed. We still need to improve the SH and extratropical surface pressure forecasts.

LETKF indicated advantages in probabilistic forecasts compared to the operational EPS. LETKF showed better brier skill scores than the singular-vector or bred-vector EPS centered at 4D-Var analysis in shorter leads up to 72 hours (Fig. 3). This tendency that LETKF probabilistic forecast is advantageous in shorter leads is true for other verification measures including ROC area.

Several major upgrades have been made to the LETKF system and resulted in steady improvements. Now it is said that overall LETKF performs comparable to 4D-Var. LETKF outperforms 4D-Var in the Tropics, and slightly outperforms in the NH in general. However, further improvements are desired for extratropical surface pressure forecasts and general performance in the SH. We will continue the development to improve the LETKF performance, so that it becomes a possible operational choice in near future.

(a)

	PseaSurf	T850	Z500	Wspd850	Wspd250
Global	−9.00	−10.45	−10.64	2.38	0.13
N. Hem.	−4.47	−2.95	−1.72	3.74	0.66
Tropics	0.48	−11.66	−17.60	11.69	9.88
S. Hem.	−10.90	−14.51	−13.00	−1.52	−3.81

(b)

	PseaSurf	T850	Z500	Wspd850	Wspd250
Global	−5.21	−2.33	−4.21	3.94	1.73
N. Hem.	−3.89	2.06	1.32	4.30	1.30
Tropics	7.05	6.49	7.44	13.58	9.57
S. Hem.	−6.35	−6.47	−6.20	0.39	−1.14

Fig. 2. Relative improvements (%) of 1- to 9-day forecast anomaly correlations of LETKF over 4D-Var, averaged over 31 days in August, 2004. Positive values indicate that LETKF outperforms 4D-Var. (a) and (b) show the cases without and with the adaptive bias correction for satellite radiances, respectively.

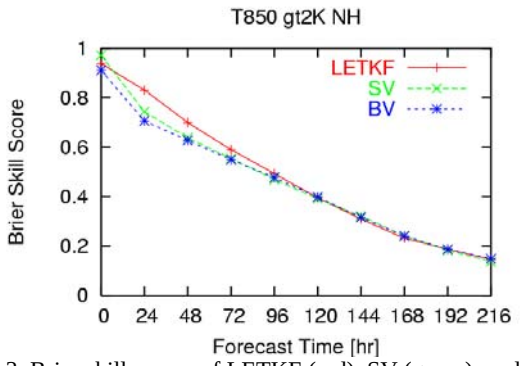

Fig. 3. Brier skill scores of LETKF (red), SV (green), and BV (blue) for the event that temperature at 850 hPa is greater than 2 K than climatology.

References

Hunt, B. R., E. J. Kostelich and I. Szunyogh, 2007: Efficient Data Assimilation for Spatiotemporal Chaos: A Local Ensemble Transform Kalman Filter. *Physica D*, **230**, 112-126.

Kadowaki, T, 2005: A 4-Dimensional Variational Assimilation System for the JMA Global Spectrum Model. *CAS/JAC WGNE Research Activities in Atmospheric and Oceanic Modelling*, **34**, 1-17.

Kalnay, E., and co-authors, 1996: The NCEP/NCAR 40-Year Reanalysis Project. *Bulletin of the American Meteorological Society*, **77**, 437-471.

Miyoshi, T and Y. Sato, 2007: Applying a local ensemble transform Kalman filter to the JMA global model. *CAS/JAC WGNE Research Activities in Atmospheric and Oceanic Modelling*, **36**, 1-11.

Miyoshi, T. and Y. Sato, 2007: Assimilating Satellite Radiances with a Local Ensemble Transform Kalman Filter (LETKF) Applied to the JMA Global Model (GSM). *SOLA*, **3**, 37-40.

Miyoshi, T., S. Yamane, and T. Enomoto, 2007: Localizing the Error Covariance by Physical Distances within a Local Ensemble Transform Kalman Filter (LETKF). *SOLA*, **3**, 89-92.

Onogi, K., and co-authors, 2007: The JRA-25 Reanalysis. *J. Meteor. Soc. Japan*, **85**, 369-432.

Sakai, R. and co-authors, 2008: A new operational one-week ensemble prediction system at JMA, this issue.

Sato, Y., 2007: Introduction of variational bias correction technique into the JMA global data assimilation system. *CAS/JAC WGNE Research Activities in Atmospheric and Oceanic Modelling*. **36**, 1-19.

Whitaker, J. S., T. M. Hamill, X. Wei, Y. Song and Z. Toth, 2007: Ensemble Data Assimilation with the NCEP Global Forecast System. *Mon. Wea. Rev.*, in press.

Increase of ATOVS radiance data in the JMA global data assimilation system in 2007

Hiromi Owada
Numerical Prediction Division, Japan Meteorological Agency
1-3-4 Otemachi, Chiyoda-ku, Tokyo 100-8122, JAPAN
E-mail: howada@naps.kishou.go.jp

JMA ingested additional ATOVS radiance data in the global data assimilation system in 2007.

AMSU-A and MHS from NOAA18 satellite, and those from Metop-A were introduced in April 2007, and in November 2007, respectively. The cycle experiments to assess the effects of these new satellite data showed the positive impacts on forecast skills in terms of the 500hPa geopotential height (data not shown).

AMSU-A, AMSU-B and MHS radiances from the Asia-Pacific Regional ATOVS Retransmission Service (A-P RARS) were added in February 2007. A-P RARS ATOVS data are directly received at stations in Japan, Australia, China and Korea, and distributed to NWP centers via GTS in a short time in order to meet the data cut-off time of early analysis (2h20m). Figure 1 shows the difference between the early analysis and the cycle (delayed) analysis of 20hPa geopotential height at 06UTC on 25 September 2006. The large negative (positive) difference is colored with blue (red). With A-P RARS data in Fig.1(b), the early analysis is closer to the delayed analysis, which is believed to be more reliable because the sufficient data is available due to its longer cut-off time length (5h35m for 00 and 12 UTC and 11h35m for 06 and 18 UTC), compared with Fig.1(a). The amount of available data, on average, increases by a factor of 1.1 to 1.4. Furthermore, the EUMETSAT Advanced Retransmission Service (EARS) ATOVS data were added in August 2007 as they were proved to have positive impacts on the analysis and the forecast for 500hPa geopotential height in the Northern Hemisphere in the impact studies.

(a) without A-P RARS

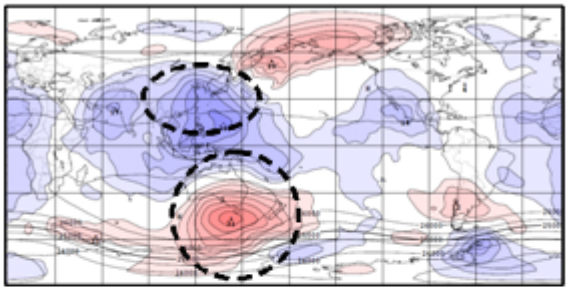

(b) with A-P RARS

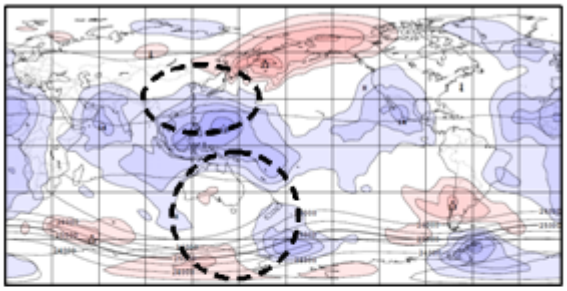

(c) NOAA15+16/AMSU

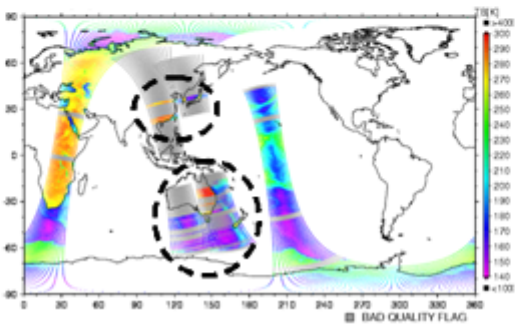

Fig.1 Difference between the early analysis and the cycle (delayed) analysis of 20hPa geopotential height (at 06UTC on 25 September 2006) without A-P RARS data of Beijing and Melbourne (a), and with A-P RARS data (b). The blue (red) shades show the positive (negative) value of the difference, and the contour interval is 4m. (c) is the coverage of Beijing and Melbourne (circled area).

Current developments on global satellite data assimilation at Météo-France

Florence Rabier, Paul Poli, Vincent Guidard, Nadia Fourrié, Elisabeth Gérard, Fatima Karbou, Patrick Moll, Christophe Payan,

CNRM/GAME, Météo-France and CNRS
42 av Coriolis
31057 Toulouse
France
Florence.Rabier@meteo.fr

Variational assimilation is a good algorithmic framework for an efficient use of satellite data of different kinds. Since 2000, an increasing number of satellite data has been used operationally in the global 4DVAR assimilation system, and a lot of progress has been achieved on the quality of the forecast. Figure 1 shows the weights of the various data-types in constraining the global analysis as of September 2007. The degrees of freedom for signal (DFS) indicate the importance of each observing system in the various regions. As expected the Northern mid-latitude troposphere is well covered by conventional observations (radiosondes and aircraft), while the stratospheric analysis relies primarily on brightness temperatures collected by satellite sounders.

In that respect, data from the AMSU-A, AMSU-B, HIRS, AIRS (a few channels) and SSM/I instruments are assimilated under the form of raw brightness temperatures. Very recently, ATOVS data from the European MetOp satellite have been inserted (5 September 2007). Different types of satellite winds (cloud winds or water vapour winds) are used, mainly from geostationary satellites but also including the MODIS winds over the poles (from the polar orbiting satellites NASA Eos-AQUA and TERRA). Scatterometer winds from the QuikSCAT satellite were introduced in October 2004, and complemented very recently by the ERS-2 winds (5 September 2007). It is worth highlighting the recent works and developments on the GPS applications in meteorology at Météo-France. On September 5th 2007, GPS radio-occultation measurements in the form of bending angles from 8 satellites were introduced in the global 4DVAR: 6 FORMOSAT-3/COSMIC satellites, plus GRACE-A and CHAMP. The assimilation experiments performed in Fall 2006, Spring and Summer 2007 showed a very significant impact of this new data type on the forecast skill for almost all the meteorological fields and all the expected areas, especially on the Southern Hemisphere. Figure 1 illustrates the importance of GPS radio-occultation measurements in constraining the analysis in the high southern latitudes where very few other observations with high vertical resolution are available.

Systematic biases of brightness temperatures are currently corrected using a Harris and Kelly (2001) scheme, which is based on a multiple linear regression against meteorological predictors (layer thicknesses, total column water vapour, surface temperature, etc.), beside corrections due to geometric matters (powers of the scan angle). This method was used in a static way, which needs a several-week period to train the regression. An adaptive method was developed and implemented at ECMWF (Auligné *et al*., 2007), which introduces the coefficients of the multiple linear regression in the control variable of the 4D-VAR. As the correction is done adaptively, it does not attempt to correct model-induced biases. Another strength of the method is that conventional data (radiosondes data in particular) act as anchors when the coefficients evolve during the minimization, which prevents insidious drifts. Météo-France benefited from ECMWF developments and introduced the variational bias correction (VarBC) in ARPEGE for all AMSU-A, AMSU-B, HIRS, AIRS and SSM/I channels, in pre-operational mode. Figure 2 illustrates the positive impact of the variational bias correction on forecast RMS with respect to radiosonde geopotential measurements, especially in the stratosphere, which lasts all along the forecast range. Our future efforts in satellite data assimilation will be geared towards the implementation of this variational bias correction for all brightness temperature sounding data, the full use of the MetOp instruments (GRAS, IASI, and ASCAT), and a global increase in the number of pieces of information actually assimilated.

References:

Harris, B. A. and G. Kelly, 2001: “A satellite radiance-bias correction scheme for data assimilation”, Q.J.R. Meteorol. Soc., 127, 1453-1468.

Auligné, T., A. P. McNally and D. Dee, 2007: "Adaptive bias correction for satellite data in a numerical weather prediction system", Q.J.R. Meteorol. Soc., 133, 631-642.

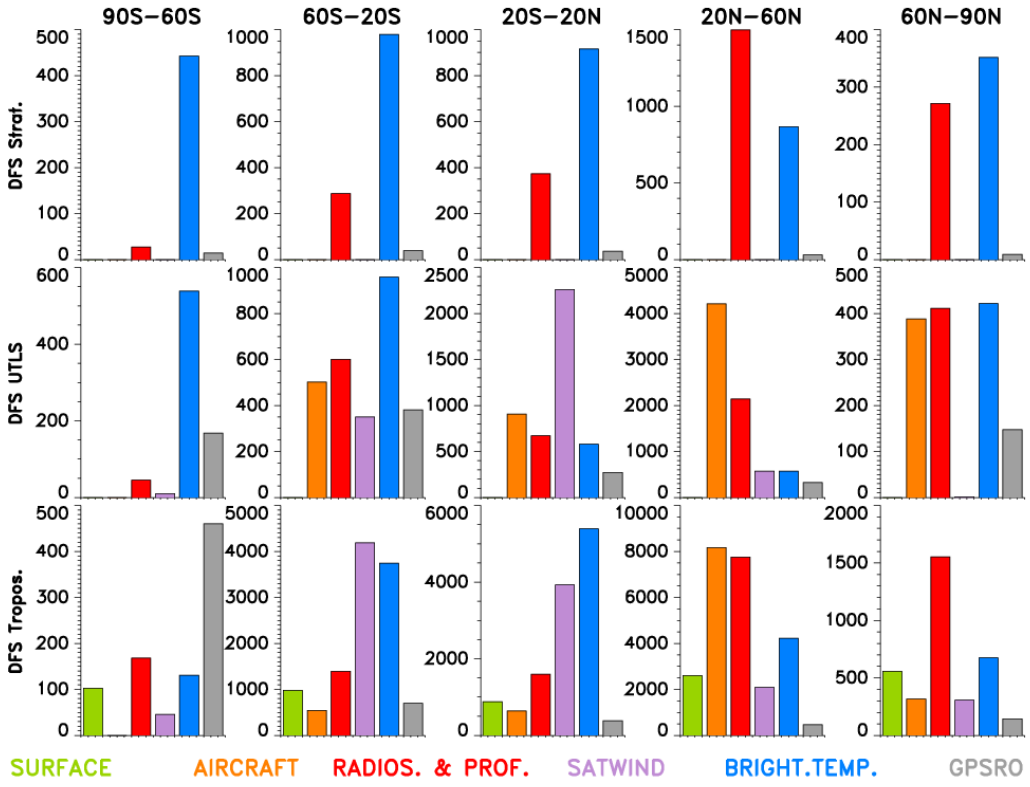

Figure 1: The numbers of degrees of freedom for signal (DFS) in the Météo-France 4DVAR analysis, as a function of observation data-type for five zonal regions and for three altitude bands (below 9 km altitude, between 9-16 km altitude, and above 16 km altitude). Note the different scales. Surface data from SYNOP, SHIP, Buoys and GPS Zenith total delays are in green, AIRCRAFT data are in orange, radiosonde and profiler data are in red, satellite winds from geostationary satellites, scatterometers and polar MODIS winds are in purple, radiance brightness temperatures from ATOVS, AIRS and SSM/I instruments are in blue, GPS radio-occultation data are in grey.

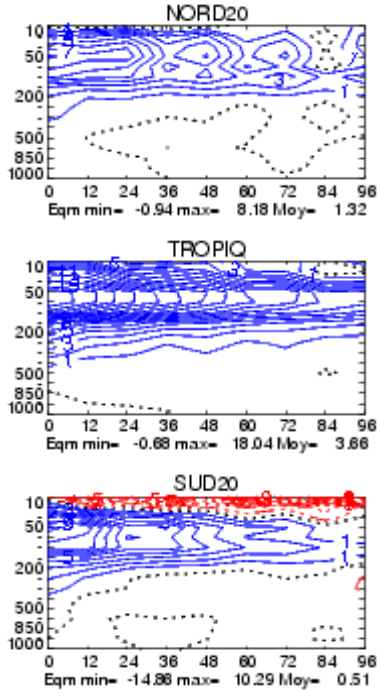

Figure 2 : RMS forecast error differences in geopotential height between the experiment using VarBC and the experiment not using VarBC, with respect to radiosonde data. RMS error differences are represented as a function of forecast range and pressure. Results are averaged over a 43 day period, in July-August 2007. Blue contours mean that VarBC improves the scores. The contour spacing is 1 m. Three areas are represented: the Northern Hemisphere (top panel), the Tropics (middle panel) and the Southern Hemisphere (bottom panel).

Mesoscale Ensemble Prediction experiment for WWRP Beijing Olympic 2008 RDP -- 2007 preliminary experiment --

Kazuo Saito*, Hiromu Seko*, Masaru Kunii*, Masahiro Hara*
Tabito Hara and Munehiko Yamaguchi****
** Meteorological Research Institute, Tsukuba, Ibaraki 305-0052, Japan; ksaito@mri-jma.go.jp*
*** Numerical Prediction Division, Japan Meteorological Agency*

The WWRP Beijing Olympic 2008 Forecast Demonstration / Research and Development Project (B08FDP/RDP) is an international research project for a short range forecast of the WMO World Weather Research Programme (WWRP), which succeeds the Sydney 2000FDP. The B08FDP/RDP is divided into two components; the FDP component for a short range forecast up to 6 hours based on the nowcasting, and the RDP component for a short range forecast up to 36 hours based on the mesoscale ensemble prediction system (MEPS). Aims of the project are to improve understanding of the high-resolution probabilistic prediction processes through numerical experimentation and to share experiences in the development of the real-time MEP system. Collaborating with JMA, the Meteorological Research Institute (MRI) has been participating in the RDP component since 2006.

In 2007, a preliminary experiment for B08RDP was conducted from 24 July to 31 August by six participants; MRI/JMA, NCEP, Meteorological Service of Canada (MSC), Austrian Zentral Anstalt fur Meterologie und Geodynamik (ZAMG), National Meteorological Center of the China Meteorological Administration (NMC/CMA) and the Chinese Academy of Meteorological Sciences of CMA (CAMS/CMA). Intercomparisons of 36 hour EPS forecast with a horizontal resolution of 15 km were conducted, and the forecast products were uploaded on the website of the B08RDP (http://www.b08rdp.org) in near real time base.

Specifications of the 2006 and 2007 experiments are listed in Table. 1. In 2007, a version of the JMA nonhydrostatic model (NHM; Saito et al., 2007a) as of May 2007 is employed as for the forecast model, where the turbulent closure model, trigger functions in the Kain-Fritsch convection scheme and the atmospheric radiation scheme have been modified. The domain has been enlarged from 221 x 201 grids of the 2006 experiment (Saito et al., 2007b) to 232 x 200 grids and shifted westward (Fig. 1), so that the southwestern corner of the verification domain is not embedded in boundary relaxation layers (24 grids = 360 km).

Initial condition of the control run is given by the JMA operational regional analysis, while for the initial perturbations, the targeted moist global SV method (T63L40) is employed in 2007, replacing the simple downscaling method of the JMA operational one-week EPS (global BGM method with TL159L40) used in the 2006 experiment (WEP). This global SV method (GSV) was originally developed at JMA for new operational typhoon EPS, while the final norm is targeted to the common verification area in B08RDP. The Lanczos method using TL/ADJ models of the JMA operational global-4DVAR is employed. Figure 2 shows time sequence of ensemble spreads for surface conditions with WEP and GSV. Spreads with GSV increase more rapidly compared with WEP. RMSEs of ensemble means by GSV are also smaller than those by WEP (figure not shown). As for the lower boundary condition, initial perturbations are evaluated using a statistical relationship between perturbations of the soil temperature and the atmospheric lowest level temperature, and are added to the 4 layer soil temperatures.

Results of the 2007 experiment were verified comparing with ground stations and sonde data. Performance of MRI/JMA products were relatively good in general for surface conditions in terms of RMSEs of ensemble mean, while following shortcomings were found. 1) Convective rains are underestimated. 2) Maximum temperatures in very hot days (>35C) are underestimated. 3) Spreads are still smaller compared with the forecast errors.

Toward the 2008 experiment, modifications of the forecast model, implementation of the lateral boundary perturbation method, test of new/revised initial perturbation methods, and application of meso-4DVAR analysis to the Beijing area (Kunii et al., 2008) are underway.

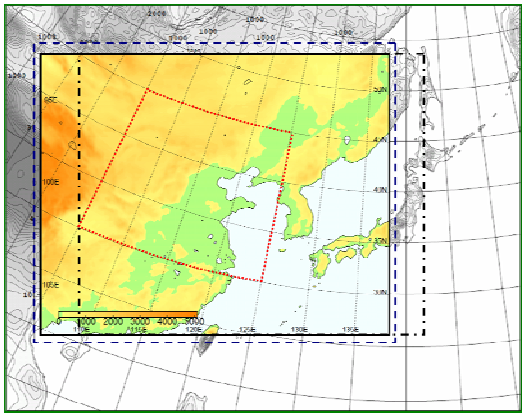

Fig. 1. Domain of the MRI/JMA 2007 experiment (colored rectangle). Fan-shaped sector over east China indicates the domain of the common verification area (105°E-125°E, 30°N-45°N) in B08RDP. Rectangle with black broken lines shows the domain of the 2006 experiment. Rectangle with blue broken lines is the domain of the Meso 4D-Var analysis for the 2008 experiment.

Table 1. Specifications of the 2006 and 2007 MEP experiments by MRI/JMA.

	2006 Experiment	2007 Experiment
Forecast model	NHM as of March 2006	NHM as of May 2007
Horizontal grid	221×201 (Δx = 15km), Lambert comformal projection	232×200 (Δx = 15km), Lambert comformal projection
Vertical grid	Terrain-following, 40 levels, Δz=40-1180m、 H=22km	No changes
Number of members	11 members	No changes
Initial condition	JMA operational regional 4D-Var (20 km resolution)	No changes
Initial perturbation	JMA one-week global EPS (TL159)	Targeted moist global SV (T63L40)
Lateral boundary	JMA RSM forecast (no perturbation)	No changes
Soil temperatures	4 layer prognostic soil temperatures	4 layer prognostic soil temperatures, Initial perturbations are added

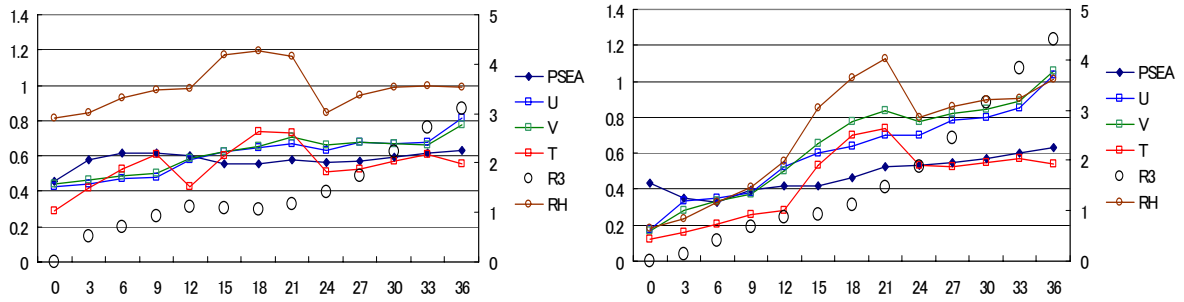

Fig. 2. Time sequence of ensemble spreads for surface conditions (PSEA; sea level pressure, U and V; 10m winds, T; 2m temperature, R3; 3 hour accumulated rain, RH; 2m relative humidty). Unit on the vertical axis is hPa for PSEA, m/s for U and V, degree for T, mm for R3 and % for RH. Verification period is 5 days from 2 to 6 July 2007. Left) Wep. Right) Gsv.

References

Kunii, M., K. Saito and H. Seko, 2008: Assimilation of Precipitation Data in Beijing Area. *CAS/JSC WGNE Research Activities in Atmospheric and Oceanic Modelling.* **38**. (submitted)

Saito, K., J. Ishida, K. Aranami, T. Hara, T. Segawa, M. Narita and Y. Honda, 2007a: Nonhydrostatic atmospheric models and operational development at JMA. *J. Meteor. Soc. Japan.*, **85B**, 271-304.

Saito, K., H. Seko, M. Kunii, T. Hara, M. Kyouda and M. Yamaguchi, 2007b: Preliminary Mesoscale Ensemble Prediction experiment for WWRP Beijing 2008 RDP. *CAS/JSC WGNE Research Activities in Atmospheric and Oceanic Modelling.* **37**, 5.25-5.30.

Japan area ensemble forecast using NHM-LETKF

*Hiromu Seko (MRI/JMA), Takemasa Miyoshi (NPD/JMA),
Masaru Kunii (MRI/JMA), and Kazuo Saito (MRI/JMA)

1. Introduction In WWRP Beijing 2008 Research and Development Project (B08RDP), inter-comparison of meso-scale ensemble forecast have been conducted. In the preliminary experiments of B08RDP, initial perturbations produced by normalizing the perturbation of operational one-week ensemble forecast (Saito, 2006) or by the global SV method were used. Besides these methods for initial perturbation, the performance of the perturbation produced by LETKF methods will be investigated. As the preliminary experiment, influences of the horizontal grid interval and horizontal resolution of observation data over the results of ensemble forecast are investigated.

2. Outline of ensemble experiments To investigate the influence of the grid interval and horizontal resolution of observation data, grid interval of 50km and 20km and observation data for global analysis (horizontal resolution 120km) and mesoscale model (20km) were used. From among the combination of the grid interval and observation data, following three experiments were performed; 50km-GA, 50km-MA and 20km-MA. Whole assimilation period is 12UTC 13th to 00UTC 17th August 2006. Period of one assimilation window is set to 6hours.

3. Results of ensemble experiment

a. Difference from observation data Number of observation data for GSM and MSM are 900-3800, 8000-16000, respectively, although the number of observation data varied with time (fig. 1). Figure 2 shows the RSM against the observation data. RMS from observation data in 20km-MA is much larger than those of 50km-GA and 50km-MA, especially in surface pressure and horizontal wind. When the experiment of 50km-GA and 50km-MA are compared, RMS of GA is slightly larger than that of MA, and RMS was gradually increased with time because the typhoon was approaching to Japan (fig. 2a and b). In 20km-MA, correction due to the assimilation of data became smaller with time (fig. 2c).

b. Horizontal distribution of ensemble mean and spread. Figure 3 shows the ensemble mean distribution of surface pressure and horizontal wind at the end of the assimilation, 00UTC 17th. The typhoons were reproduced in all experiments. However, when GA data was assimilated, pressure at the center of typhoon was larger and the weak rainfall region became wider. When the MA data was assimilated with the 20km-grid model, Typhoon was most developed and the depression of the center pressure became closer to the best truck data.

As for the spread, spreads in the experiments of 50km-GA and 50km-MA were large, although the spread at the boundary was small because the boundary was fixed (fig. 4). In 50km-GA, the spread was largest, and high spread region was seen on the southern part of typhoon. In the 20km-MA and 50km-MA, in which large number of observation data were assimilated, spread was smaller, and high spreads were seen only near the center of the typhoon. This difference seems to be caused by the resolution of the assimilated data.

4. Summary When the grid interval of 50 k m was used, GA data was not sufficient for the assimilation data.]When MA data of which data resolution is 20 km was used, the typhoon was developed, although the central pressure of the typhoon was still larger than the observed one. From these experiments, the proper resolution of observation data is needed to obtain the realistic analyses fields.

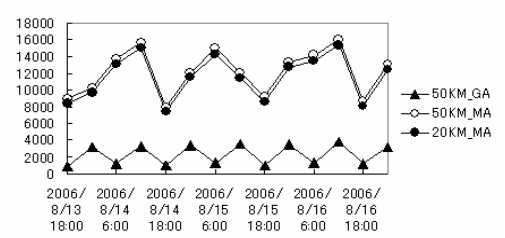

Fig. 1 Number of assimilation data at each cycle

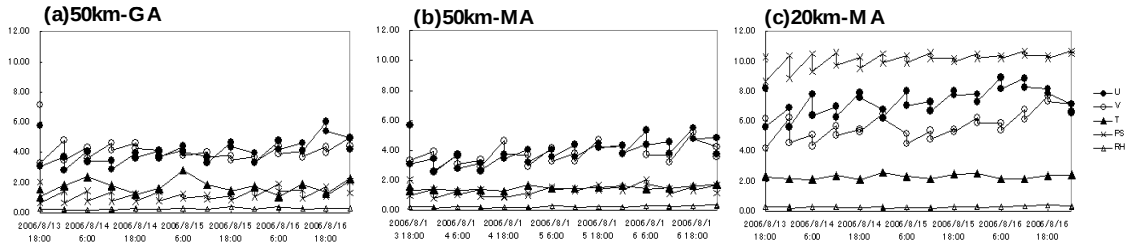

Fig. 2 Temporal variation of RMS in 50km-GA, 50km-MA and 20km-MA at each assimilation cycle. RMS was obtained from forecasted and analyzed values and the observation data

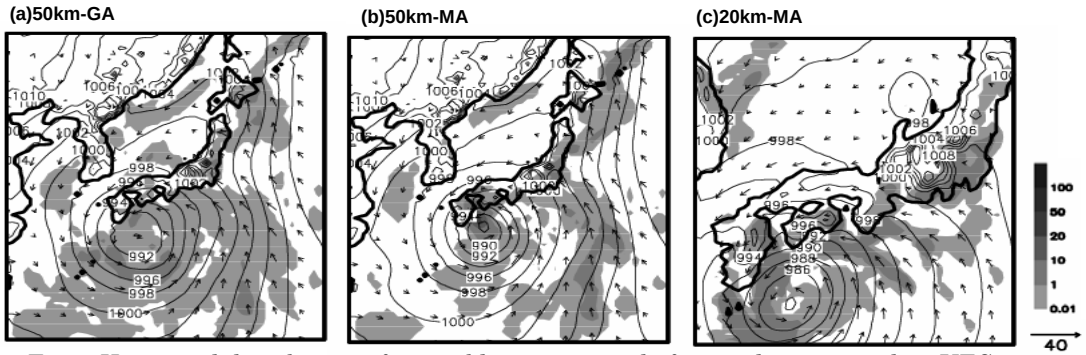

Fig. 3 Horizontal distribution of ensemble mean at end of assimilation period, 00UTC 17 August 2006. Shadow regions, contour and vectors indicate the rainfall, surface pressure and horizontal wind, respectively.

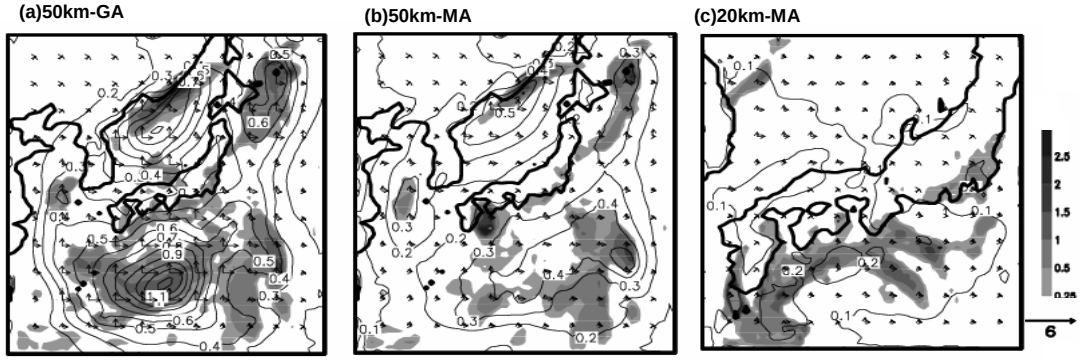

Fig.4 Horizontal distribution of ensemble spread at the end of assimilation period, 00UTC 17 August 2006. Shadow regions, contour and vectors indicate the rainfall, surface pressure and horizontal wind, respectively.

Assimilation experiments using COSMIC occultation data

Hiromu Seko*, Yoshinori Shoji*, Masaru Kunii*
Jun-ichiro Furumoto, and Toshitaka Tsuda ****
** Meteorological Research Institute, Tsukuba, Ibaraki 305-0052, Japan*
*** Research Institute for Sustainable Humanosphere, Kyoto University*

1. Introduction Radio wave transmitted from GPS satellites is bended or delayed when it penetrated the atmosphere. The bending angle and atmospheric delay have the information of atmosphere along the path from GPS satellite and Low Earth Orbit (LEO) satellite. In GPS occultation observation, vertical profile of refractivity can be obtained from the bending angle or atmospheric delay. In MRI, the assimilation method for the GPS occultation data has been developed by using the occultation data observed by LEO satellite CHMAP, and the impact of it on the rainfall forecasts has been investigated with Meso-4Dvar system of JMA. On June 2006, new LEO satellite COMIC, which is composed of 6 satellites, was launched. In this report, the impact of COSMIC data is investigated using the developed method.

2. COSMIC occultation data Figure 1a shows the horizontal distribution of the tangent point, which is the closest point to the earth on the path, from 1st to 14th September 2006. These data were provided by UCAR, which is one of the organizations that have developed the COSMIC. Because the COSMIC is composed of 6 satellites, number of the occultation data is much larger than that of CHAMP. The observed refractive index ($n=(N-1)*10^6$) that existed in the domain of meso-scale model (MSM) of JMA was compared with the first-guess index produced from the outputs of MSM (fig. 1b). Refractivity index was estimated from the lower height than the CHAMP data, and the bias of the difference between aforementioned indexes is as small as that of CHAMP data. Thus, COSMIC data is expected to be useful assimilation data.

3. Outline of assimilation methods Assimilation method that was developed with CHAMP data was used. In this method, the path data, not tangent point data, is assimilated in consideration of the vertical correlation of the observational error. When CHAMP occultation data, of which tangent point passed near the rainfall system, was assimilated, the rainfall system, which was not developed when CHAMP data was not assimilated, was well reproduced. Because the rainfall forecast was improved and the property of the occultation data (i.e. path data and vertical correlation of the observation error) was considered, this methods seems to be one of proper assimilation method.

4. Assimilation results There were 10 profiles estimated from the lower layer in the domain of MSM (fig.1c). In most of the profiles, the difference of first-guess and observed indexes at lowest height was positive. These positive differences at northern and central Japan and North Korea are expected to moisten the atmosphere when these data are assimilated. On the other hand, there was a profile whose lowest difference is negative on southeast of Japan.

Figure 2a shows the difference of water vapor between the analyses, which were estimated with and without the assimilation of path data. Water vapor was increased at the central and northern Japan and North Korea. The water vapor was decreased where the refractive index with negative difference was observed. This increment of water vapor indicates that the assimilation was performed correctly. When the forecast was performed from this analysis field, the rainfall region over the central Japan was expanded (fig. 3). The rainfall region extending from central Japan to northeast, which is marked by circles, becomes closer to the observed one. This result indicates that COSMIC data improves the rainfall forecast.

Finally, the difference of impact of the tangent point data and path data are explained. Figure_2b shows the difference of water vapor from the control run with the assimilation of path data or tangent point data. There is a large difference of the increment near North Korea. In this area, conventional data reduced the moisture near North Korea. When the tangent point was assimilated, the water vapor only around tangent point was increased. On the other hand, water vapor along the path line indicated red line was moistened by the assimilation of occultation data. This difference indicates that path data should be assimilated.

tangent point data. There is a large difference of the increment near North Korea. In this area, conventional data reduced the moisture near North Korea. When the tangent point was assimilated, the water vapor only around tangent point was increased. On the other hand, water vapor along the path line indicated red line was moistened by the assimilation of occultation data. This difference indicates that path data should be assimilated.

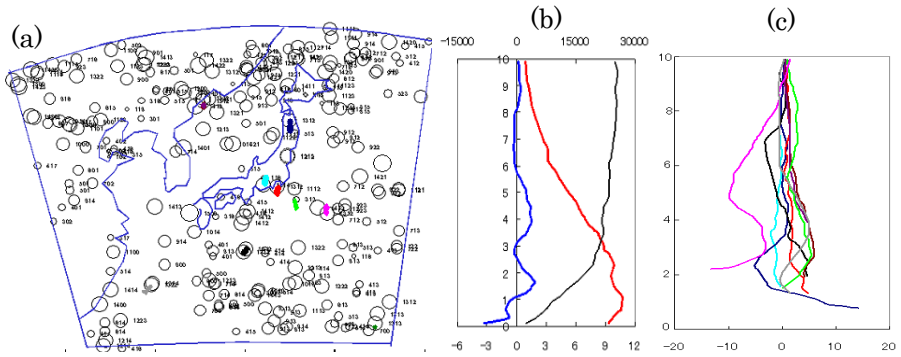

Fig. 1: (a) Distribution of tangent point observed by COSMIC from 1 to 14 September 2006. (b) Vertical distribution of bias and RMS of 'D-values'. Thin line indicates the number of the occultation data. (c) vertical distribution of D-values observed from 21JST to 24JST 13 September 2006.

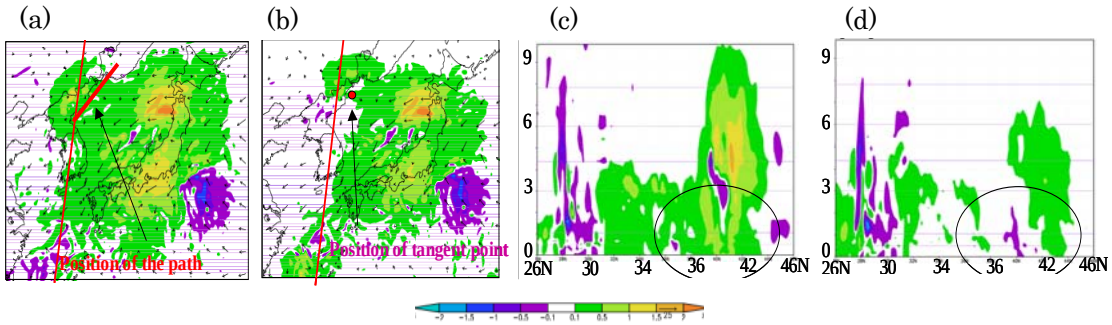

Fig. 2 Difference of water vapor of analysis fields from that of the control run. Path data (a) and tangent point data (b) were assimilated, respectively. (c) and (d) are the cross section along the red line in (a) and (b)

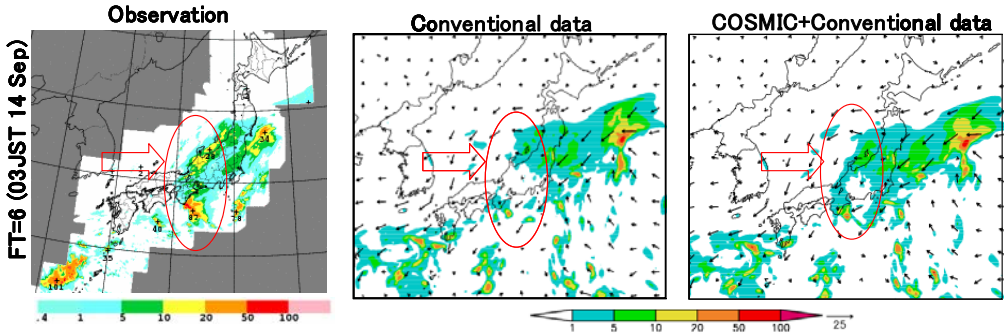

Fig. 3: (Left) Rainfall observed by conventional radar and rain gauges from 00JST to 03JST 13 September 2006. (Center) Rainfall distribution predicted from analyzed fields that were obtained by the assimilation of conventional data (CNTL). (Right) Same as except for by assimilation of conventional data and COSMIC data.

Meso-ensemble experiments on potential parameter of tornado formation using JMANHM

Hiromu Seko*, Kazuo Saito*, Masaru Kunii*
Tabito Hara, and Munehiko Yamaguchi****

** Meteorological Research Institute, Tsukuba, Ibaraki 305-0052, Japan*
*** Numerical Prediction Division, Japan Meteorological Agency*

1. Introduction Tornados with Fujita scale of 2 and 3 occurred in Japan in 2006, and caused severe disasters. Numerical simulations have been performed with cloud-resolving model to investigate the structure and formation mechanisms of tornados (e.g. Tsuboki, 2007; Mashiko, 2007; Kato 2007). Besides the simulation of the tornados, the forecast and warning system of tornados is developed by the JMA. In this system, potential of tornado formation is predicted by the deterministic forecast. However, the forecast does not always express the real state of atmosphere because the initial field of numerical forecast includes the analysis error. In ensemble forecast, many perturbations that have the property of atmosphere (e.g. large perturbation near the disturbance) are added to the initial fields, and then numerical forecasts are performed from these initial fields. It is statistically known that ensemble means becomes closer to the actual atmosphere. Moreover, probability that the parameter, such as CAPE, exceeds some threshold can be obtained from the many forecasts of ensemble members. The oversights of the severe weather become fewer when the forecasts of ensemble member are used. Therefore, ensemble forecast is expected to be useful to reduce the impact of the disaster. With collaborating with Japan Meteorological Agency (JMA), Meteorological Research Institute participates WWRP Beijing 2008 project (hereinafter, Beijing project), and develops the mesoscale ensemble forecast system. In this study, the techniques, which have been developed in the Beijing project, is applied to the parameters of tornado formation to show the usefulness of ensemble forecast.

2. Specification of ensemble experiment The numerical model and the initial perturbation producing method are the same as those of Beijing project. The domain of the model is set to be 3300 km x 3000 km. The horizontal grid interval is 15 km. The initial perturbation was produced by adding the normalized perturbation of one-week ensemble of JMA to the initial fields of the JMA regional spectrum model (RSM) (Saito et al, 2006). In this report, potential parameters of two tornado case events were investigated. First case is F2 tornado occurred in Kyushu (southernmost main island of Japan) on 17 September. Another is F3 tornado occurred in Hokkaido (northernmost main island of Japan) on 6 November 2008. Initial times of the ensemble forecasts are 12UTC of previous days. Figure 1 shows the surface pressure and rainfall region of the control run, which was the prediction from the initial condition without adding any disturbances. Typhoon and low-pressure system, in which the tornados occurred, were reproduced in both forecasts. Because the positions of the simulated typhoon and low-pressure system are similar to the observed ones, the environment (e.g. vertical shear) around the tornadoes is expected to be well reproduced in the control run forecast.

3. Results of ensemble experiment Figures 2 and 3 show the probability distributions of storm relative helicity (SReH), CAPE and product of CAPE and SReH that exceeds 25, 1000 and 30000, respectively. CAPE is the parameter that indicates how intense convection can be generated. SReH indicates how intense vorticity is produced by the low-level airflows. The product of CAPE and SReH, which corresponds to the parameter of EHI, indicates both effects.

In the first case, there were high probability areas, in which SReH exceeds 25, in the central part of Japan on northeast of the center of Typhoon (fig. 2). On the other hand, high probability that CAPE exceeds 1000 existed on the south of western part of Japan. In both distributions, there are excess regions of high probability on central part of Japan and on the southern side of Japan, respectively. As for the products of CAPE and SReH, the region that probability of this product exceeding 30000 is more than 50% remained at only the eastern part of Kyushu. This result indicates that the ensemble forecast is useful, when the product of CAPE and SReH is used as potential parameter of the tornado formation.

Can products of CAPE and SReH be well forecasted in the second case? Figure 3 shows the same as the fig. 2 except but the date of the forecast. High probability region in which the product of CAPE and SReH exceeds 30000 remained at the eastern Hokkaido. This result supports the usefulness of the ensemble forecasts.

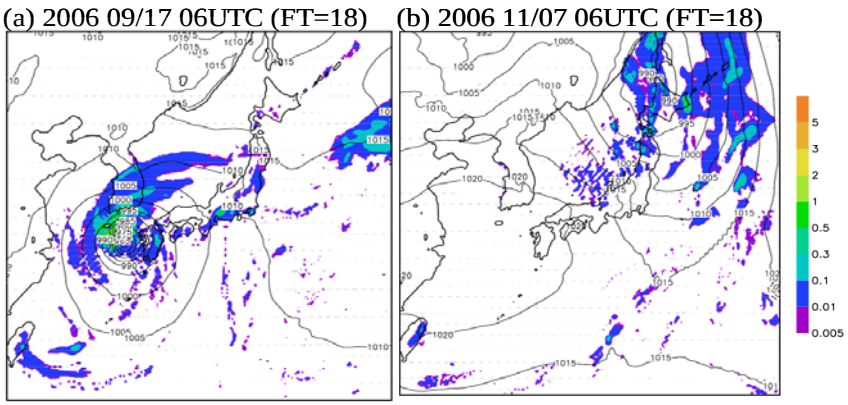

Fig. 1 Horizontal distribution of mixing ratio of rain water at the lowest level of JMANHM at 06UTC 17 Sep 2006 and 06UTC 7 November 2006. Counter lines indicate the sea surface pressure.

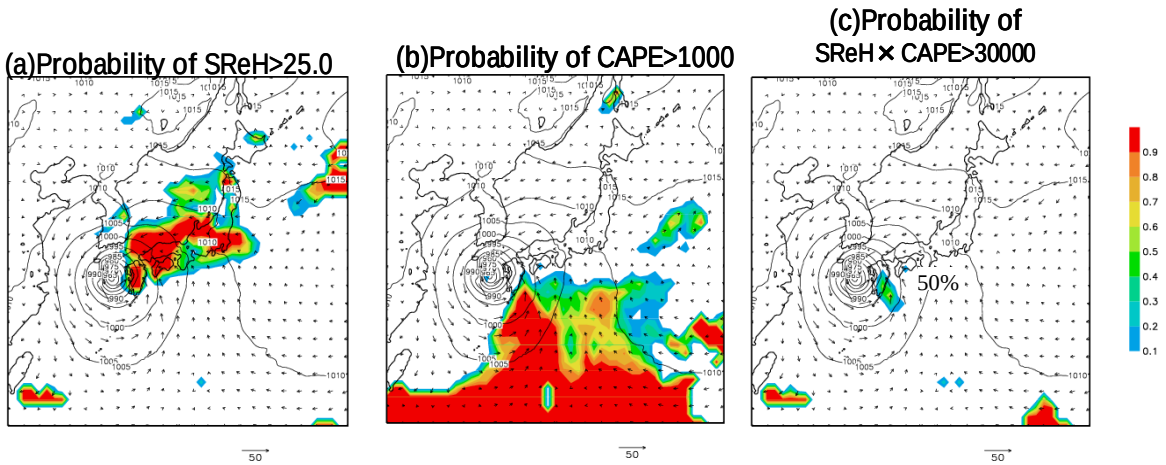

Fig. 2 Probability of (a) SReH, (b) CAPE and (c) SReH*CAPE exceeding to 25.0, 1000, and 300000, respectively. These probabilities were produced from output of ensemble forecast at 06UTC 17 September 2006.

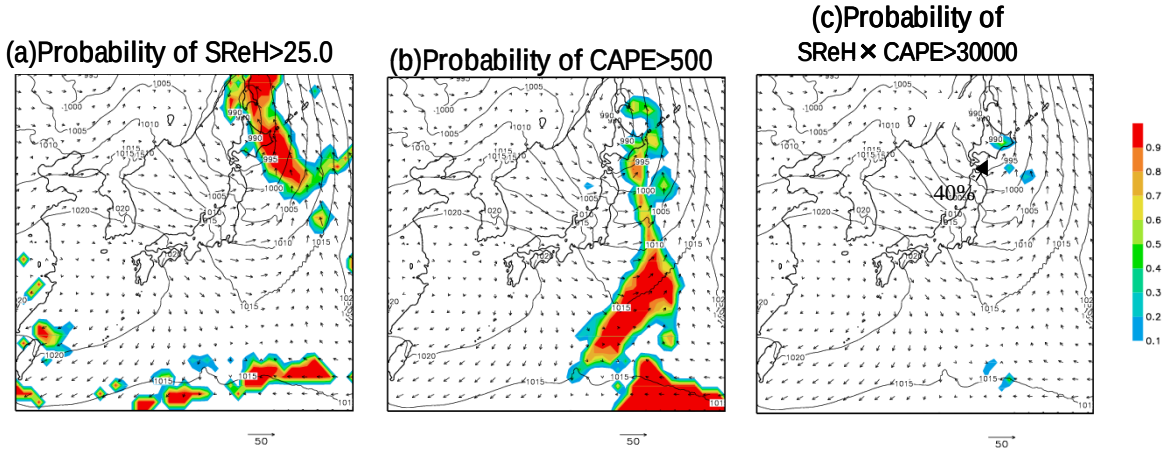

Fig.3 Same as fig.2 except for at 06UTC 7 November 2006.

Tier-2 downscale experiments of B08RDP

Hiromu Seko, Kazuo Saito, and Masaru Kunii
Meteorological Research Institute, Tsukuba, Ibaraki 305-0052, Japan; hseko@mri-jma.go.jp

1. Introduction In WWRP Beijing 2008 Forecast Demonstration Project /Research and Development Project, intercomparison on the forecasts with the cloud resolving model of the horizontal grid interval of 2-3km (Tier-2) is performed, besides Tire-1 experiment that is the mesoscale ensemble forecast with the grid interval of 15km. Targets of the Tier-2 experiment is the severe phenomena occurred in Beijing area. Squall line developed over the Beijing city on 1st August 2006 and thunderstorm on 30th July 2007 have been investigated so far. As for the squall line case, it was reported that the squall line was well reproduced by assimilation of ground-based GPS data by the UCAR and Beijing Meteorological Bureau (Kuo et al. 2007). We performed the downscale experiments with the non-hydrostatic model with the grid interval of 3km model on the thunderstorm occurred on 30 July. In this report, the results of this downscale experiment are explained.

2. Downscale experiment of thunderstorm on 30th July 2007. The convective rainfall of the thunderstorm was generated on the west of Beijing at 20LST 29th July, and then moved eastward. Radar reflectivity indicates that there are intense line-shaped bands extending from south to north embedded in the weak rainfall region. These bands kept their shape while they passed eastward. Three-hour precipitation over 70mm/3hour was observed near the Beijing city when this thunderstorm passed.

Mesoscale ensemble forecast was applied to this intense thunderstorm case. The initial perturbation was produced by normalizing the initial perturbation of operational one-week ensemble forecast to the scale of the analysis error of Meso-4Dvar system of JMA (Saito et al. 2006). The downscale experiments with the grid interval of 3km were performed from the initial fields, which were produced from 10 ensemble members and one control run. Figure 1 shows the rainfall regions of which rainfall was strongest (M05m) and weakest (M02p) among the ensemble members, in addition to the control run (M00). The line-shaped band was reproduced in members of M05m and CNTL. The line-shaped band was produced by the

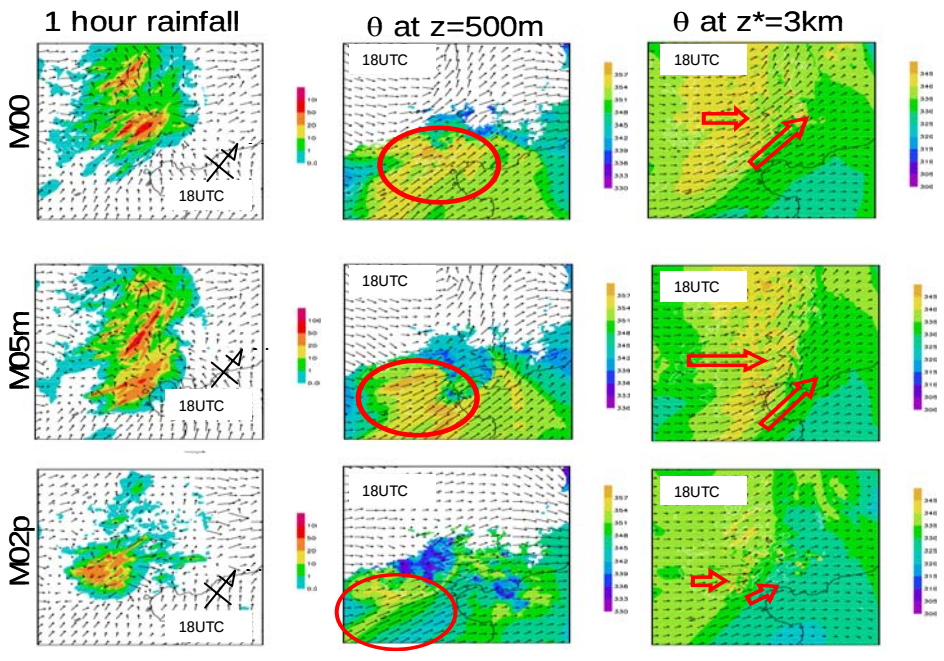

Fig. 1 Horizontal distribution of 1-hour rainfall, equivalent potential temperature at z=500m and 3km at 18UTC

convergence of the low-level inflow from the south and the cold pool. The convective cell was generated on the southern tip of the band, and then moved northward by the airflow above the height of 3km. The generation point and movement of convective cells is one of factors that determine the shape of the rainfall system. When M05m was compared with CNTL, equivalent potential temperature of the low-level inflow is higher, and the westerly flow penetrated at the height of 3km. This airflow enhanced the evaporation of the rain droplets, and then produced the intense cold pool. On the other hand, the rainfall was relatively weak and a line shaped band was not organized in M02p. Equivalent temperature was lower than CNTL. These results indicate that the environment that was different in each member produced the different type of rainfall system.

3. Comparison with Tire-1 experiments Does these downscale experiments have more information than the Tier-1 has? The grid point data with the interval of 15km was produced from output of Tier-2, and then compared with the result of Tire-1. Shapes of the rainfall system produced in Tier-2 experiments were similar to those of Tier-1 (fig.2). The boundary condition of Tire-2, which was produced by the interpolation of the output of Tier-1, determines the position of the intense convergence. The environment of Tier-2 was also similar to that of Tier-1. Thus the similar shape and type convective systems are produced. Next, rainfall amount of Tier-2 is compared with Tier-1. Rainfall amount was also similar to that of Tier-1 expect M04p (fig. 3). The rainfall amount was also controlled by the boundary condition. On the other hand, the maximum rainfall amount is larger than that of Tier-1. The rainfall region exceeding 1mm/3hour is smaller than Tier-1. These results indicated the rainfall region of Tier2 is more localized. This feature is confirmed by the histogram of rainfall. Namely, higher ranked rainfall of Tier-2 was larger than that of Tier-1. Heavy rainfall was often caused by slow moving rainfall system. Thus, the maximum rainfall is more important to forecast the heavy rainfall. The relationship between the environment and localization of the rainfall should be investigated.

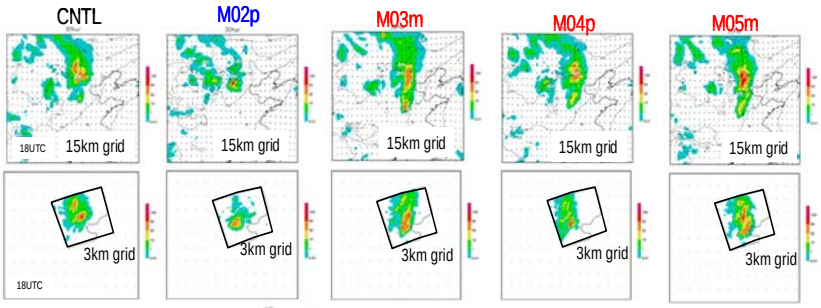

Fig.2 3-hour rainfall distribution of Tier-1 and Tier-2. Rectangular in lower panels indicate the model domain of Tier-2.

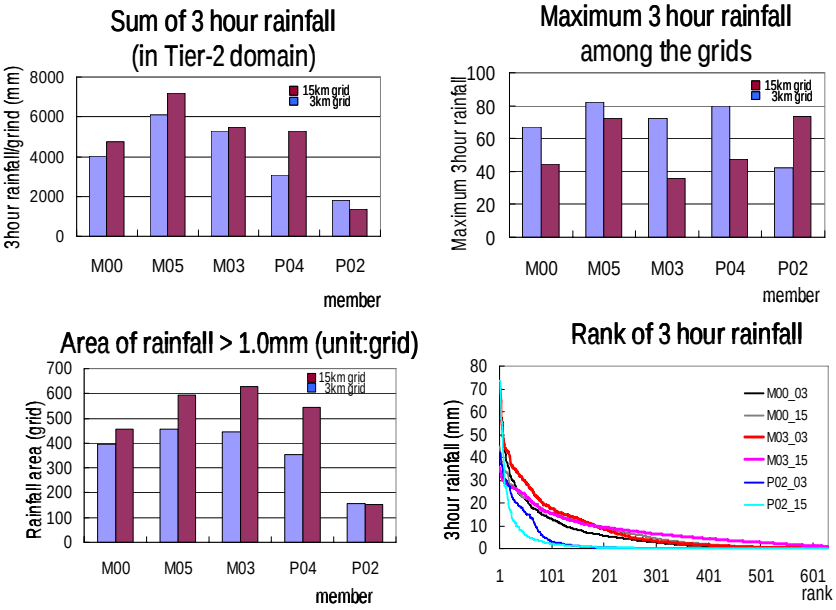

Fig. 3 Sum of 3-hour rainfall (upper left), maximum rainfall (upper right) and area exceeding 1mm/3hou (lower left) of Tier-1 and Tier-2. Histogram of the 3hour-rainfall (lower right)

New 2-Meter Relative Humidity Analysis for SL-AV model

A. Shlyaeva[1], *M. Tolstykh*[1,2]
e-mail: shlyaeva@gmail.com, tolstykh@inm.ras.ru
[1] Hydrometeorological Research Center of Russia, Moscow, Russia
[2] Institute of Numerical Mathematics, Russian Academy of Sciences, Moscow, Russia

The global semi-lagrangian NWP model SL-AV [1] was developed in Hydrometeorological Research Center of Russia and Institute of Numerical Mathematics, Russian Academy of Sciences. The horizontal resolution of the model is 0.9° in longitude and 0.72° in latitude; currently there are 28 vertical levels. Subgrid scale parametrizations developed in Meteo-France for ARPEGE/IFS [2] model are used.

Recently, subgrid scale parametrization of the surface physical processes ISBA [3] has been implemented [4] in the model. The assimilation of soil variables was implemented according to [5]. This assimilation scheme uses 2 meter temperature (for brevity denoted as T2m) and relative humidity (RH2m) increments for yielding soil variables increments. It is straightforward that accurate and reasonable T2m and RH2m analysis is required.

Due to lack of accuracy in the existing analysis [6], new RH2m analysis was implemented for SL-AV model. The analysis uses SYNOP and SHIP observations. First guess of the analysis is SL-AV 6-hour forecast starting from the previous assimilation step.
The method used is the optimal interpolation, the algorithm is similar to those implemented in ECMWF [7] and HIRLAM [8]. The background covariance matrix depends not only on the distance between the points but also on the orography difference of the considering points.

Number of the observations that might be assimilated at each gridpoint is restricted to 50. Land / sea observations are used only for assimilation over land / sea.

It is known that analysis which does not take into account possible correlations between observations could increase analysis error in regions with high density of observations [9]. It is also known that optimal thinning could extract all necessary information from the observations. Averaging of the neighboring observations is a good alternative to thinning as it saves more information about observations. In the considered analysis in case of close observations (i.e. observations that are closer to each other than the prespecified distance set to 30 km) “superobservation” is generated which is simple average of these observations.

The implementation of analysis allows manipulation with the values of the e-folding distances that can be different for different latitude bands and as well for the land and the sea.

The experiments were carried out in order to determine the standard deviations of background and observation errors. As a result their values were set to 0.12 and 0.1 respectively.

Table 1 contains biases and root-mean square errors (RMS) of the implemented analysis (new) and previously used analysis (old) errors with respect to the observations averaged for November 2007. Obviously, new analysis significantly reduces biases and RMS errors of the RH2m analysis.

Table 1

	Bias (new)	Bias (old)	RMS (new)	RMS (old)
Central part of Russia	0,003	0,034	0,060	0,088
Europe	0,007	0,038	0,080	0,098
Asia	-0,001	-0,077	0,095	0,150
Russia	0,001	-0,047	0,082	0,128
Siberia	0,001	-0,054	0,079	0,123

RH2m analysis was also implemented for SL-AV model version with variable resolution grid [10]. The latitude spacing in this version is varying from 30 km over 48-90º N to 70 km in the southern hemisphere. Longitude spacing is 0.5625° ensuring horizontal resolution over Russia to be about 30 km. Table 2 contains biases and root-mean square errors of the first guess (FG) and implemented analyses for the variable resolution grid (var) and regular grid (reg) errors with respect to the observations. The statistics is averaged over November 2007. Previously used analysis is out of consideration because it was not adapted for the variable resolution grid.

Table 2

	Bias (FG)	Bias (var)	Bias (reg)	RMS (FG)	RMS (var)	RMS (reg)
Central part of Russia	-0,066	0,004	0,003	0,114	0,058	0,060
Europe	-0,048	0,005	0,007	0,130	0,077	0,080
Asia	0,019	0,002	-0,001	0,170	0,095	0,095
Russia	-0,007	0,002	0,001	0,146	0,081	0,082
Siberia	0,000	0,003	0,001	0,129	0,078	0,079

One can observe that the results of the analysis for the variable resolution grid are similar to those for the regular grid.

Introduction of the described RH2m analysis alone with recently developed T2m 2DVAR analysis and ISBA implementation [11] resulted in the improvement of the T2m and RH2m SL-AV model forecasts. The considered RH2m analysis for SL-AV model is used operationally since June 2007.

References

1. Tolstykh M. Semi-Lagrangian high resolution model of the atmosphere for numerical weather prediction. – Russian Meteorology and Hydrology, 2001, N4 , pp. 1-9.
2. Geleyn, J.-F., Bazile, E., Bougeault, P. et al. Atmospheric parameterization schemes in Meteo-France's ARPEGE N.W.P. model. - In “Parameterization of subgrid-scale physical processes”, ECMWF Seminar proceedings, 1994, pp. 385-402.
3. Noilhan J. and Mahfouf J.-F. The ISBA land surface parameterisation scheme. – Global Planet. Change, 1996, Vol 13, pp. 145 – 149.
4. Bogoslovskii N.N., Tolstykh M.A., Implementation of assimilation scheme for soil variables in the global semi-Lagrangian NWP model, Computational Technologies, 2006, V.11, Special issue ENVIROMIS-2006, part 3, pp. 20-25. [Russian].
5. Giard D. and Bazile E. Implementation of a new assimilation scheme for soil and surface variables in a global NWP model. - Mon. Wea. Rev., 2000, Vol 128, pp. 997-1015.
6. M.D. Tsyryulnikov, M.A. Tolstykh, A.N. Bagrov, R.B. Zaripov. - Development of a global data assimilation system with variable resolution. - Russian Meteorology and Hydrology, 2003, N4, pp. 5-24.
7. IFS Documentation CY31R1. Part II: Data assimilation.
8. Navascués, B.: Analysis of 2 meter Temperature and Relative Humidity. – HIRLAM Technical Report No. 28. Norrköping, January 1997.
9. Liu, Z.-Q., Rabier. F. 2002. The interaction between model resolution and observation resolution and density in data assimilation: A one-dimensional study. Q.J.R.M.S., 128, 1367-1378.
10. Tolstykh M.A. Variable resolution version of the SL-AV global NWP model // Russian J. Num. An. & Math. Mod. 2003. V. 18, N4. P. 347-361.
11. Bogoslovskii N.N., Shlyaeva A.V., Tolstykh M.A. Data assimilation of surface and soil variables in the global semi-Lagrangian NWP model, Computational Technologies, 2008, V.13, Special issue CITES-2007, 7 pp., accepted. [Russian].